UNIVERSIDADE DO ESTADO DE SANTA CATARINA – UDESC
CENTRO DE CIÊNCIAS TECNOLÓGICAS – CCT
PROGRAMA DE PÓS-GRADUAÇÃO – ENGENHARIA MECÂNICA

NATÁLIA KAUANA GESSER MIOTTO

ANALYSIS OF THE IMPACT OF IMPURITIES IN CO2-RICH MIXTURES IN CCS/CCUS APPLICATIONS

JOINVILLE
2025

NATÁLIA KAUANA GESSER MIOTTO

ANALYSIS OF THE IMPACT OF IMPURITIES IN CO2-RICH MIXTURES IN CCS/CCUS APPLICATIONS

Dissertação apresentada ao Programa de Pós-Graduação em Engenharia Mecânica do Centro de Ciências Tecnológicas da Universidade do Estado de Santa Catarina, como requisito parcial para obtenção do grau de mestre em Engenharia Mecânica.

Orientador: Prof. Dr. Antonio Marinho Barbosa Neto

Coorientador: Dr. Diego Tavares Volpatto

JOINVILLE

2025

Ficha catalográfica elaborada pelo programa de geração automática da Biblioteca Universitária Udesc, com os dados fornecidos pelo(a) autor(a)

Miotto, Natália Kauana Gesser
Analysis of the impact of impurities in CO2-rich mixtures in CCS/CCUS applications / Natália Kauana Gesser Miotto. -- 2025.
93 p.

Orientador: Antonio Marinho Barbosa Neto
Coorientador: Diego Tavares Volpatto
Dissertação (mestrado) -- Universidade do Estado de Santa Catarina, Centro de Ciências Tecnológicas, Programa de Pós-Graduação em Engenharia Mecânica, Joinville, 2025.

1. CO2. 2. Impurities. 3. Phase Behavior. 4. Equations of State. 5. CCS. I. Barbosa Neto, Antonio Marinho. II. Volpatto, Diego Tavares. III. Universidade do Estado de Santa Catarina, Centro de Ciências Tecnológicas, Programa de Pós-Graduação em Engenharia Mecânica. IV. Titulo.

NATÁLIA KAUANA GESSER MIOTTO

ANALYSIS OF THE IMPACT OF IMPURITIES IN CO2-RICH MIXTURES IN CCS/CCUS APPLICATIONS

Dissertação apresentada ao Programa de Pós-Graduação em Engenharia Mecânica do Centro de Ciências Tecnológicas da Universidade do Estado de Santa Catarina, como requisito parcial para obtenção do grau de mestre em Engenharia Mecânica.

Orientador: Prof. Dr. Antonio Marinho Barbosa Neto

Coorientador: Dr. Diego Tavares Volpatto

BANCA EXAMINADORA

Antonio Marinho Barbosa Neto, Dr.
Universidade do estado de Santa Catarina - UDESC

Membros:

Gustavo Gondran Ribeiro, Dr.
Universidade do Estado de Santa Catarina - UDESC

Celso Peres Fernandes, Dr.
Universidade Federal de Santa Catarina - UFSC

Joinville, 27 de Fevereiro de 2025.

AGRADECIMENTOS

Eu gostaria de expressar minha sincera gratidão à minha mãe e à minha irmã pelo apoio incondicional e por sempre estarem ao meu lado. Sou profundamente grata pelo amor e pela força que me deram. Saibam que vocês forma incrivelmente importantes para que eu chegasse até aqui.

Aos meus orientadores, por me ensinarem tanto e por me acompanharem em cada etapa. Agradeço por me compreenderem tão bem, por serem meus parceiros e por acreditarem em mim.

Ao pessoal do Thermophase, por todo o suporte ao longo desta jornada.

Muito obrigada!

RESUMO

A Captura e Armazenamento de Carbono (CCS) é uma tecnologia promissora na mitigação do aquecimento global, capturando CO_2 de fontes industriais e da atmosfera para posterior armazenando geológicas ou reutilização. A eficiência do CCS é influenciada por impurezas que alteram as propriedades do fluido, exigindo uma seleção criteriosa de equações de estado (EoS) para modelar essas misturas com precisão. Dessa forma, este estudo investiga o impacto das impurezas no comportamento de fase e a densidade de misturas ricas em CO_2 e avalia os modelos GERG-2008 e EOS-CG 2019 em suas versões originais e ajustadas, na previsão das densidades de misturas binárias ($CO_2 + CO$, $CO_2 + Ar$ e $CO_2 + CH_4$). A metodologia adotada envolveu refinamento dos parâmetros ajustáveis das equações de estado por meio da ferramenta *Thermobuilder*, além da determinação das densidades e dos envelopes de fases através de simulações no *software Multiflash.* A análise dos ajustes revelou que, na maioria dos casos, o ajuste melhorou ligeiramente a capacidade preditiva dos modelos para as densidades. No entanto, para a mistura $CO_2 + CO$, a versão ajustada da EOS-CG 2019 não trouxe melhorias, e sua versão original teve melhor desempenho em comparação com a GERG-2008 ajustada. Para o sistema $CO_2 + CH_4$, a GERG-2008 ajustada apresentou menores valores de ARE em comparação com a EOS-CG 2019 original, porém a versão desta última após o ajuste dos parâmetros teve melhor capacidade preditiva das densidades com base nos dados experimentais utilizados. Já para a mistura contendo Ar como impureza, o refinamento de ambos os modelos trouxe melhorias, mas o ajuste da EOS-CG apresentou o melhor desempenho. Além disso, foi verificado que o aumento da concentração de impurezas amplia a região bifásica no envelope de fases, deslocando os pontos críticos e reduzindo a densidade. Isso implica a necessidade, por exemplo, de maiores pressões operacionais para manter o fluxo monofásico durante o transporte da mistura rica em CO_2. Quanto à redução da densidade, o Ar tem menor influência, enquanto que o CH_4 exerce maior influência na fase líquida e menor na fase gasosa.

Palavras-chave: CO2, Impurezas, Comportamento de fases, Equações de Estado, CCS.

ABSTRACT

Carbon Capture and Storage (CCS) is a promising technology for mitigating global warming, capturing CO_2 from industrial and atmospheric sources for subsequent geological storage or reuse. The efficiency of CCS is influenced by impurities that alter the fluid properties, requiring a careful selection of equation of state (EoS) to accurately model these mixtures. Thus, this study investigates the impact of impurities on the phase behavior and density of CO_2-rich mixtures and evaluates the GERG-2008 and EOS-CG 2019 models in their original and adjusted versions, in predicting the densities of binary mixtures ($CO_2 + CO$, $CO_2 + Ar$ and $CO_2 + CH_4$). The methodology adopted involved tuning the adjustable parameters of the equations of state using the Thermobuilder tool, in addition to determining the densities and phase envelopes through simulations in the Multiflash software. The analysis of the adjustments revealed that, in most cases, the adjustment slightly improved the predictive capacity of the models for densities. However, for the $CO_2 + CO$ mixture, the tuned version of EOS-CG 2019 did not bring improvements, and its original version performed better compared to the tuned GERG-2008. For the $CO_2 + CH_4$ system, the adjusted GERG-2008 presented lower ARE values compared to the original EOS-CG 2019, but the latter's version after tuning had better predictive capacity of densities based on the experimental data used. For the mixture containing Ar as an impurity, the tuning of both models brought improvements, but the tune of EOS-CG 2019 showed the best performance. In addition, it was verified that increasing the concentration of impurities expands the two-phase region in the phase envelope, changing critical points and reducing the density. This implies the need, for example, for higher operating pressures to maintain the single-phase flow during the transport of the CO_2-rich mixture. Regarding the reduction of density, Ar has less influence, while CH_4 exerts greater influence in the liquid phase and less in the gas phase.

Keywords: CO2, Impurities, Phase Behavior, Equations of State, CCS

LIST OF ILLUSTRATIONS

Figure 1 – Atmospheric $CO2$ levels from 1750 to 2021 19
Figure 2 – Evolution of the $CO2$ capture project pipeline (number of capture facilities) 20
Figure 3 – A visual overview of each step in the CCUS process. 21
Figure 4 – Operating conditions for different processes and methods of $CO2$ transport in CCS chain presented from phase envelope of pure $CO2$. 22
Figure 5 – Example of a phase envelope for a pure substance and a binary system. CP is the Critical point. 25
Figure 6 – Diagram of the iterative process for flash calculation 27
Figure 7 – Binary interactions in GERG-2008 31
Figure 8 – Binary interactions in EOS-CG 2019 34
Figure 9 – Illustration of dataset splitting into training and validation set. 36
Figure 10 – Step by step flowchart of results 42
Figure 11 – Tuned parameters in each combination 43
Figure 12 – Synthesis of tune results analyses 43
Figure 13 – Ranking of the EoS selection that presented the best error values for validation data for each mixture. 46
Figure 14 – Density behavior for the $CO2 + CO$ mixture at 273.15 K. 47
Figure 15 – Density behavior for the $CO2 + CO$ mixture at 300.15 K. 47
Figure 16 – Density behavior for the $CO2 + CO$ mixture at 353.15 K. 48
Figure 17 – Density behavior for the $CO2 + Ar$ mixture at 273.15 K. 50
Figure 18 – Density behavior for the $CO2 + Ar$ mixture at 300.15 K. 50
Figure 19 – Density behavior for the $CO2 + Ar$ mixture at 353.15 K. 51
Figure 20 – Density behavior for the $CO2 + CH4$ system at 273.15K. 51
Figure 21 – Density behavior for the $CO2 + CH4$ system at 300.15K. 52
Figure 22 – Density behavior of systems with 5% of impurity at 300.15 K. 53
Figure 23 – Phase envelope for $CO2 + CO$ mixture. 54
Figure 24 – Phase envelope for $CO2 + Ar$ mixture. 55
Figure 25 – Phase envelope for $CO2 + CH4$ mixture. 55
Figure 26 – Phase envelope of $CO2$-rich mixture with 5% of impurity. 57

LIST OF TABLES

Table 1 – Summary of $CO2$ impurities from different $CO2$ capture technologies. 23
Table 2 – Helmholtz equations of state used for the pure components in the EOS-CG 2019 mixture model. 32
Table 3 – References of analyzed experimental data. 35
Table 4 – Summary of experimental density data considered for each of the mixture studied. 36
Table 5 – Investigated combinations of tuning parameters. 37
Table 6 – Summary of model and tuning performance for validation set. The best results are highlighted in bold. Calculated errors based on density values. 44
Table 7 – Model validity ranges by mixture. 45
Table 8 – MAE values ($kg/m3$) comparing the density of pure $CO2$ with the densities of mixtures containing CO at 300.15 K for phase. 48
Table 9 – MAE values ($kg/m3$) comparing the density of pure $CO2$ with the densities of mixtures containing CO at different molar fraction and temperatures. . 49
Table 10 – MAE values ($kg/m3$) comparing the density of pure $CO2$ with the densities of mixtures at different concentrations and temperatures. 52
Table 11 – MAE values ($kg/m3$) comparing the density of pure $CO2$ with the densities of mixtures at 300.15 K for phase. 53
Table 12 – Effect of impurities on density reduction compared to pure $CO2$ at 300.15 K. 54
Table 13 – Critical points for different concentrations of CO, Ar and $CH4$. 56

LIST OF ABBREVIATIONS AND ACRONYMS

API	Application Programming Interface
ARE	Absolute Relative Error
CCS	Carbon capture and storage
CCUS	Carbon capture, utilisation and storage
DAC	Direct Air Capture
EOR	Enhanced oil recovery
EoS	Equation of State
EOS-CG	Equation of State for Combustion Gases and Combustion Gas like Mixture
GERG	Groupe Européen de Recherches Gazières
GHG	Greenhouse Gas
IBP	Instituto Brasileiro de Petróleo
ID	Identification Code
IPCC	Intergovernmental Panel on Climate Change
ISO	International Organization for Standardization
MAE	Mean Absolute Error
RMSE	Root Mean Square Error

LIST OF SYMBOLS

CO_2	Carbon Dioxide
O_2	Dioxygen
Ar	Argon
CO	Carbon Monoxide
CH_4	Methane
N_2	Nitrogen gas
No_x	Nitrogen oxides
SO_2	Sulfur dioxide
SO_3	Sulfur trioxide
H_2O	Water
H_2S	Hydrogen sulfide
H_2	Hydrogen gas
COS	Carbonyl sulfide
F_{ij}	Weighting factor for binary generalized departure functions
F	Feed molar flow rate
f	Fugacity
G	Gibbs free energy
K	Equilibrium ratio or K-factor
R	Universal gas constant
P	Pressure
T	Temperature
$\bar{x}$	Molar composition
x	Mole fraction in the liquid phase
y	Mole fraction in the gas phase
z	Component mole fraction in the feed
α	Helmholtz free Energy
a^o	Ideal gas part of the Helmholtz free Energy
a^r	Residual part of the Helmholtz free Energy
α_{oi}^o	Dimensionless form of the Helmholtz free energy in the ideal gas state
α_{oi}^r	Residual part of the reduced Helmholtz free energy

$\Delta\alpha^r$	Departure function of the reduced Helmholtz free energy
γ	Binary parameter of residual part of the reduced Helmholtz free energy
ρ	Density
δ	Reduced density
τ	Inverse of the reduced temperature
φ	Fugacity coefficients
μ	Chemical potential
μ^o	Reference chemical potential

LIST OF SUPERSCRIPTS AND SUBSCRIPTS

c	Property at critical point
i	Referring to component i
ij	Interaction of component i with component j
j	Referring to component j of a binary mixture
ji	Interaction of component j with component i
k	Binary interaction parameter
L	Referring to liquid phase
N	Number of the mixture components
r	Referring to reduced property
T	Temperature
V	Referring to vapor phase
v	Volume

SUMÁRIO

1 INTRODUCTION 14
1.1 MOTIVATION 16
1.2 OBJECTIVES 16
1.2.1 General Objective 16
1.2.2 Specific Objectives 16
2 CARBON DIOXIDE AND CCS/CCUS SYSTEMS OVERVIEW 18
2.1 CARBON DIOXIDE 18
2.2 CCS/CCUS 20
3 MATERIALS AND METHODS 24
3.1 PHASE EQUILIBRIUM 24
3.1.1 Flash calculation 25
3.1.2 Fugacity 27
3.2 THERMODYNAMIC MODELING 28
3.2.1 GERG-2008 formulation 28
3.2.2 EOS-CG 2019 formulation 32
3.3 DATA COLLECTION 34
3.4 SIMULATIONS IN MULTIFLASH 36
3.4.1 Data preprocessing 36
3.4.2 Tuning of the models 37
3.4.3 Phase envelopes 38
3.4.4 Densities 39
3.5 STATISTICAL ANALYZES 39
4 RESULTS AND DISCUSSIONS 41
4.1 COMPARISON OF FITTING RESULTS 43
4.2 INFLUENCE OF IMPURITIES ON DENSITY AND PHASE ENVELOPE . 46
4.2.1 Effect of impurities on density 46
4.2.2 Effect of impurities on phase envelope 54
5 CONCLUSION 58
5.1 FUTURE RESEARCH SUGGESTIONS 59
5.1.1 Model optimization and tuning 59
5.1.2 Physical-informed Neural Networks approach 59
5.1.3 Applications in CCS and CCUS 60

REFERENCES.....61
APPENDIX A - CARBON DIOXIDE + CARBON MONOXIDE SYSTEM ($CO2 + CO$)
.....66
APPENDIX B - CARBON DIOXIDE + ARGON SYSTEM ($CO2 + Ar$).....77
APPENDIX C - CARBON DIOXIDE + METHANE SYSTEM ($CO2 + CH4$).....86

1 INTRODUCTION

Global average temperatures have risen by approximately 1ºC between 1850 and 2019 (Wang et al., 2023), an increase largely attributed to human activities driving the accumulation of greenhouse gases (GHG), formed mainly by carbon dioxide, in the atmosphere (EPE, 2018).

To limit this increase to below 2°C above pre-industrial levels, 196 countries have signed the Paris Agreement committing to GHG emission reductions and investing in climate change mitigation measures (Brasil, 2018).

The industrial sector, particularly the oil industry, plays a crucial role in achieving this goal. Many companies are looking for Net Zero strategies, investing in renewable energy and low-carbon technologies, including carbon capture and storage (CCS) and the carbon capture, utilization and storage (CCUS) (Wang et al., 2023).

The Brazilian Petroleum Institute (IBP) (2023), considers CCUS one of the main (if not the most) technologies in combating global warming caused by anthropogenic factors. It involves capturing and separating CO_2 from industries or atmosphere sources, compressing it into a supercritical fluid for transport, and then either permanently storing it (CCS) in geological formations or depleted oil reservoirs, or temporarily storing it for reuse in applications like enhanced oil recovery (EOR) or energy generation.

The carbon capture method employed influences the purity of the resulting CO_2 gas, as each method produced different impurities (Porter et al., 2015). In general, the presence of impurities in CO_2-rich mixtures can alter the fluid's properties and phase behavior compared to pure CO_2. These changes can affect density, viscosity, and phase transitions, potentially complicating the design and operation of CCS processes. Impurities can also shift temperatures and pressures conditions, leading to phase separation, increased pipeline corrosion risk, and reduced efficiency in compression and injection stages. Therefore, careful management of impurities is essential for effective CCS implementation (Wetenhall et al., 2014).

This research studies specifically mixtures involving $C0_2$ in combination with CO, Ar and CH_4. Carbon monoxide is a toxic gas that, at certain

concentrations, can cause health and environmental problems. Furthermore, it can react with other components, causing corrosion in pipelines and equipment, which can increase the risk of leaks and accidents (James, 2019). CO as an impurity arises in the CCS chain during the carbon capture stage, mainly through the pre-combustion method (Porter et al., 2015).

Argon as an impurity arises primarily in the oxy-combustion process during the CO_2 capture stage, as it can form from excess oxidant used for combustion (Porter et al., 2015). Argon, as a noble, inert gas that does not react with CO_2 or pipeline and equipment materials under operating conditions, the primary risks associated with its presence relate to changes in the physical properties of the mixture (Yu et al., 2025).

Methane is highly flammable. At high temperatures, especially within pressurized systems, the risk of explosion increases significantly in the presence of a spark. CH_4 arises in the CCS chain primarily during pre-combustion (Porter et al., 2015).

Consequently, understanding the influence of these contaminants on fluid behavior is crucial. Aside from physical experiments, thermodynamic modeling provides an alternative to evaluate and get insights on phase behavior and volumetric properties. This kind of approach employs equations of state (EoS) that are capable of accurately modeling CO_2-rich mixture containing impurities.

While widely used, cubic equations of state like Peng-Robinson often struggle to accurately predict properties near the critical point, a region of special importance in CCS applications (McKay et al., 2022). This limitation arises from the simplifying assumptions made in Peng-Robinson's derivation, causing discrepancies in the predicted behavior, especially for complex mixtures and conditions far from ideal gas behavior.

Multi parameter EoS, such as GERG-2008 and EOS-CG 2019, generally offer superior accuracy for predicting vapor-liquid equilibrium and density in CO_2-rich mixtures (Lozano-Martín et al., 2020). While these models provide good predictions, they can be fine-tuned to enhance their accuracy and ensure safer and more efficient design of CCS facilities.

1.1 MOTIVATION

Impurities can significantly increase the cost associated with CO_2 processing, transportation and storage, while also posing additional challenges to design, operation, health and safety, and system integrity. Therefore, understanding the influence of the main impurities is of great importance for the industry, especially for the proper sizing and design of CCS processes.

A comprehensive understanding of how impurities in CO_2-rich mixtures affect the CCS process chain requires interdisciplinary contributions to enable process simulations, geological surveys, materials science, and safety analyses. At some point all these efforts require accurate knowledge of the thermodynamic properties of the mixtures involved.

1.2 OBJECTIVES

1.2.1 General Objective

This dissertation aims to evaluate the performance of multiparameter equations of state to predict the density and phase behavior of CO_2-rich mixture with relevant impurities in the context CCS/CCUS.

1.2.2 Specific Objectives

To achieve the general objective, the following specific objectives are proposed:

- Identify the main impurities present in CO_2-rich mixtures and how they arise during CCS/CCUS processes;
- Compile a database of experimental density data for mixtures under investigation, sourced from relevant scientific literature.
- Review and understand the main multiparameter equations of state used in the industry for modeling CO_2-rich mixtures;

- Investigate and fine-tune the parameters of key equations of state, employing Multiflash and Thermobuilder software, to improve the accuracy of density prediction;
- Analyze the impact of impurities on the density and phase envelope in operational conditions of CCS/CUSS processes;

2 CARBON DIOXIDE AND CCS/CCUS SYSTEMS OVERVIEW

2.1 CARBON DIOXIDE

Carbon dioxide is a molecule composed of one carbon atom and two oxygen atoms (CO_2), connected by covalent bonds. Under normal conditions of temperature and pressure, it exists as a colorless and odorless gas (at low concentrations), making it difficult to detect in most environments.

While CO_2 is typically a gas, it can become a liquid at pressures above 0.51795 MPa and temperature above 216.592 K. However, at pressures and temperatures exceeding 7.3773 MPa and 304.1282 K, respectively, CO_2 reaches a critical density of 467.6 kg/m³ and transforms into a supercritical fluid, that is, this state exhibits properties intermediate between those of a liquid and a gas (Span & Wagner, 1996a).

Carbon dioxide is naturally found in low concentrations in the atmosphere. It is produced through respiration by various organisms, volcanic eruptions, and the decomposition of organic matter (eCycle, n.d.).

Plants utilize this CO_2 for photosynthesis. Oceans also naturally absorb CO_2, contributing to the calcification processes of certain marine organisms. The presence of low concentrations of CO_2 in the atmosphere is essential for maintaining a temperature and climate suitable for living on Earth.

However, as illustrated in Figure 1, CO_2 emissions have increased exponentially since the Industrial Revolution in the 18th century. Key contributing factors include the burning of fossil fuels, agricultural and industrial activities that release carbon dioxide into the atmosphere, and deforestation, which reduces natural CO_2 absorption.

The primary concern is not the mere presence of CO_2, but rather its large increased atmospheric concentration. Largely due the human activities, this elevated concentration is driving global temperature increases beyond ideal levels, ocean acidification, and glacial melt, disrupting the balance of ecosystems.

Figure 1 – Atmospheric CO_2 levels from 1750 to 2021

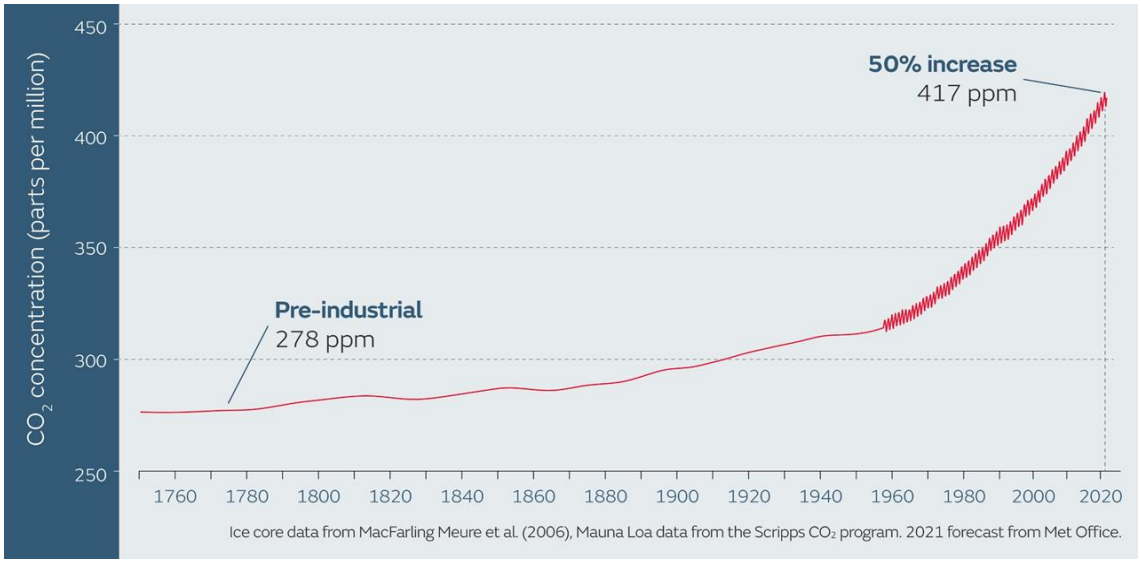

Source: Betts and Keeling (2021).

Over the years, several international agreements have been established to reduce greenhouse gases emissions. The most recent one, the Paris Agreement, aims to limit global warming to no more than 2ºC above pre-industrial levels, while also encouraging these efforts to be intensified to restrict the increase to 1.5°C by 2100 (Brasil, 2018).

In addition to the Paris Agreement, another very well-known is the Kyoto Protocol. It fostered the development of the international carbon market, which allows countries that emit CO_2 below their assigned target to sell excess emission allowances (carbon credits) to countries exceeding their limits. Consequently, a carbon credit (equivalent to one ton of carbon dioxide) is now traded as a commodity in this market (SEBRAE, 2023).

The carbon market is one of several initiatives designed to reduce CO_2 emission. Another important tool employed by high-emitting industries is Carbon Capture and Storage/Utilization (CCS/CCUS). The oil industry, with its existing experience in CO_2 separation, transport and reinjection within CCUS processes, is particularly well-positioned to benefit from this technology. CCS/CCUS can be used to offset GHG from these industries (IBP, 2023).

2.2 CCS/CCUS

On the world stage, the capacity of CCS facilities in operation has been growing gradually since 2010, as well as those in the advanced development stage as of 2017 (Figure 2). The CCUS technology has seen remarkable growth, with significant increases in projected capture capacity (up 35%) and storage capacity (up 70%) by 2030. While this progress is promising, the number still fall short of the targets set by the Net Zero Emissions by the 2050 scenario. This highlights the need for accelerated development and implementation of CCUS technology if it's to play a crucial role in combating climate change (IEA, 2024a)

Figure 2 – Evolution of the CO_2 capture project pipeline (number of capture facilities)

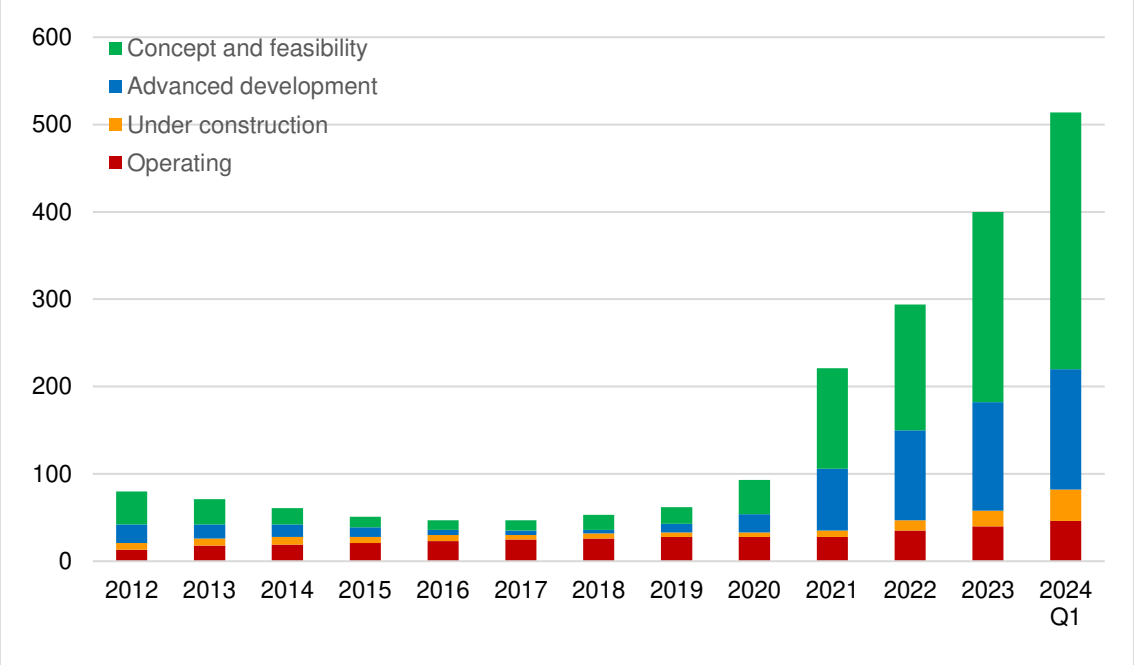

Source: Adapted from IEA (2024).

The Intergovernmental Panel on Climate Change - IPCC, (2005) emphasizes the crucial role of CCS technologies in achieving CO_2 emission reduction targets. The IPCC defines CCS as "a process consisting of the separation of CO_2 from industrial and energy-related sources, transport to a storage location and long-term isolation from the atmosphere" as illustrated in Figure 3.

Figure 3 – A visual overview of each step in the CCUS process.

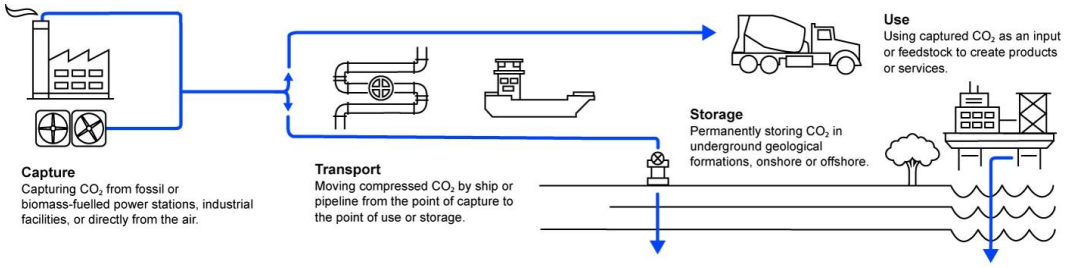

Source: Adapted from IEA, (2024a)

As previously mentioned, CCS involves three key stages: capturing CO_2, transporting it, and finally storing or utilizing it. Carbon dioxide can be captured from various sources, including power plants, industrial facilities (mainly cement and steel), refineries, and even directly from the air (known as DAC). For each of these sources there is a more suitable capture technology.

Pre-combustion capture separates CO_2 before fuel combustion by gasifying the fuel into synthesis gas, reacting it with steam, and removing the CO_2 before combustion. Post-combustion capture, on the other hand, separates CO_2 after combustion by passing the gases through an absorption equipment where a solvent captures the CO_2, which is then released for separation (Spigarelli & Kawatra, 2013). Oxy-combustion burns fuel in a high-oxygen environment, requiring an air separation unit to produce pure oxygen, which is then mixed with recycled CO_2 and used for combustion, producing a gas stream rich in CO_2 and water vapor, which is then removed (Mondal et al., 2012).

Once captured, the CO_2 is transported to storage sites, primarily via pipelines or ships. Pipeline transport typically involves compressing gaseous CO_2 to pressures above 8 MPa, and having high level of purity, to avoid two-phase flow and increase its density, making transport more efficient and cost-effective (IPCC, 2005). In addition, this compression also reduces the efforts on the compressors.

For offshore storage sites or long-distance transport, ships are often used. As Ozaki and Ohsumi (2011) describe, the CO_2 is transported via pipelines to a port and then transferred to ships. At the port, the CO_2 is liquefied, reducing its volume and allowing for larger quantities to be transported at once.

Suitable storage locations include saline formations, oil reservoirs, and aquifers. Site selection considers factors such as rock formation characteristics,

structural integrity, and geological features. The captured CO_2 is injected into these formations, where it becomes trapped within the pores or faults (Tomić et al., 2018).

The pressure and temperature at the storage site (Figure 4) determine whether the CO_2 exists in a liquid, gas, or supercritical state, facilitating its penetration into the rock pores, also depending on the wettability conditions between the rock and the fluid. This principle is also applied in EOR, where CO_2 is injected into oil wells for permanent storage and to increase oil production, the CCUS (Prasad et al., 2023).

Figure 4 – Operating conditions for different processes and methods of CO_2 transport in CCS chain presented from phase envelope of pure CO_2.

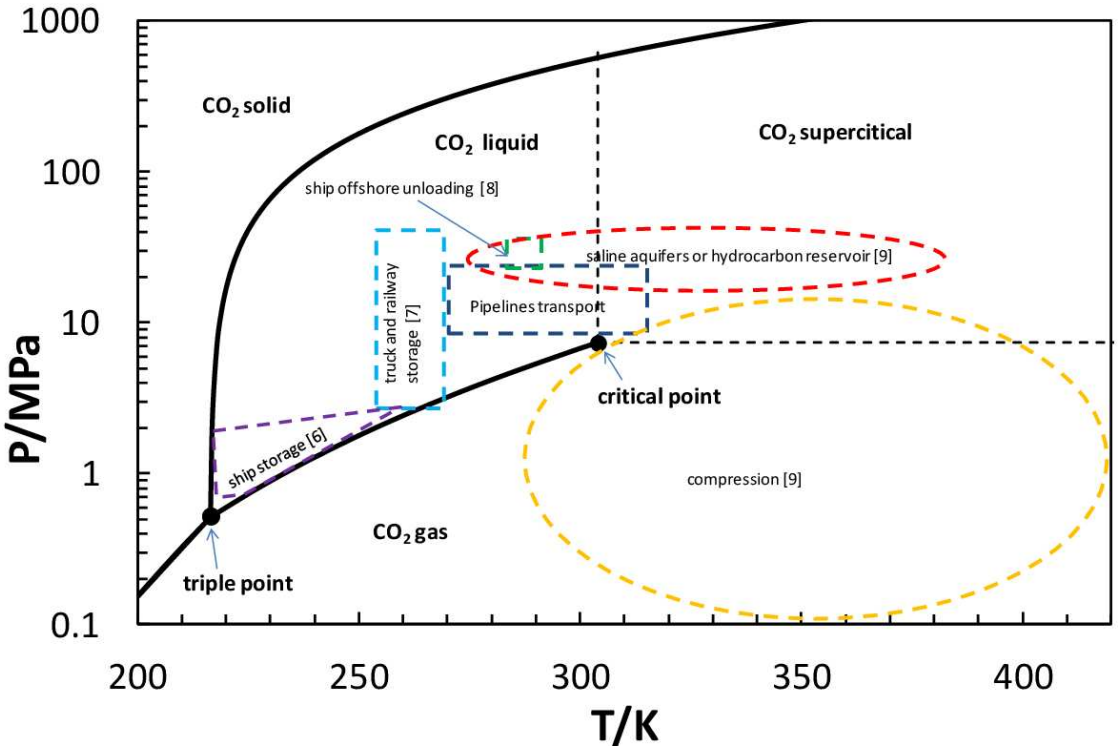

Source: AL-SIYABI (2013).

A key consideration is that impurities primarily arise during the CO_2 capture stage, where the chosen capture method directly influences both the concentration and composition of these impurities (Table 1). These impurities can affect CCS operations, from pipeline design and operation to geological storage possibilities. Because impure CO_2 streams behave differently than pure CO_2, understanding these differences is essential. Physically, impurities alter the

phase behavior and density of the CO_2. For example, non-condensable impurities like Ar, O_2, CO and CH_4, which cannot be liquefied at ambient temperatures, affect CO_2 density. These impurities, which are less compressible than pure CO_2, can also reduce system capacity when they replace pure CO_2 (Ahmad et al., 2023; Wetenhall et al., 2014).

Table 1 – Summary of CO_2 impurities from different CO_2 capture technologies.

Impurity	Oxyfuel combustion			Pre-combustion	Post-combustion
	Raw/dehumidified	Double Flashing	Distillation		
CO_2% v/v	74.8-87.0	95.84-96.7	99.3-99.95+	95-99	99.6-99.8
O_2% v/v	3.21-6.0	1.05-1.2	0.001-0.4	0	0.015-0.0035
N_2% v/v	4.0-16.6	1.6-2.03	Traço-0.2	0.0195-1	0.045-0.29
Ar% v/v	2.3-4.47	0.4-0.61	Traço-0.1	0.0001-0.15	0.0011-0.021
No_x (ppmv)	100-709	0-150	3-100	400	20-38.8
SO_2 (ppmv)	36-800	0-4500	0.1-50	25	0-67.1
SO_3 (ppmv)	20	-	0.1-20	-	N.I
H_2O (ppmv)	100-1000	0	0-100	0.1-600	100-640
CO (ppmv)	50-162	-	<2-50	0-2000	1.2-10
H_2S/COS (ppmv)				0.2-34000	
H_2 (ppmv)				20-30000	
CH_4 (ppmv)				0-112	

Source: PORTER et al. (2015).

3 MATERIALS AND METHODS

This section briefly describes the thermodynamic approach used in this work. It explains how to model phase splitting and behavior, thermodynamic models, and the strategy for fitting them. The data collection and processing are outlined, along with an overview of the experimental data used in the model calibration. The statistical metrics used in this work are introduced at the end of the section.

3.1 PHASE EQUILIBRIUM

Knowledge of a system's phase equilibrium is essential for process planning and operation. It provides valuable insights to increase efficiency, resource conservation, and safe operation. In the oil industry, for example, the phase behavior under different temperature and pressure directly impacts the transport and storage stages.

Phase equilibrium refers to the condition in which different phases of a set of chemical components coexist at equilibrium, meaning that the chemical potential of any substance is the same in all phases in which it occurs. This equilibrium is governed by the laws of thermodynamics and is essential for understanding the stability and transformation of phases under varying conditions such as temperature and pressure (Mortimer, 2000). This balance is visually represented and analyzed using a phase diagram, a graph that maps the stability of different phase as a function of pressure and temperature (Figure 4).

For a pure substance, the phase diagram consists of simple curves representing solidification, sublimation, and vaporization. However, the CO_2 used in CCS often contains impurities, primarily from the capture process, making it a mixture. These impurities alter the phase behavior compared to pure CO_2, as the properties of the additional components must be considered. The phase diagram for a mixture, sometimes called a phase envelope (for binary systems), is defined by the dew and bubble point curves, which meet at mixture's critical point. Unlike the pure substance diagram, the region within the bubble and dew curves represents a two-phase region where the phases coexist in equilibrium, as shown by Figure 5 (Mokhatab et al., 2019).

Figure 5 – Example of a phase envelope for a pure substance and a binary system. CP is the Critical point.

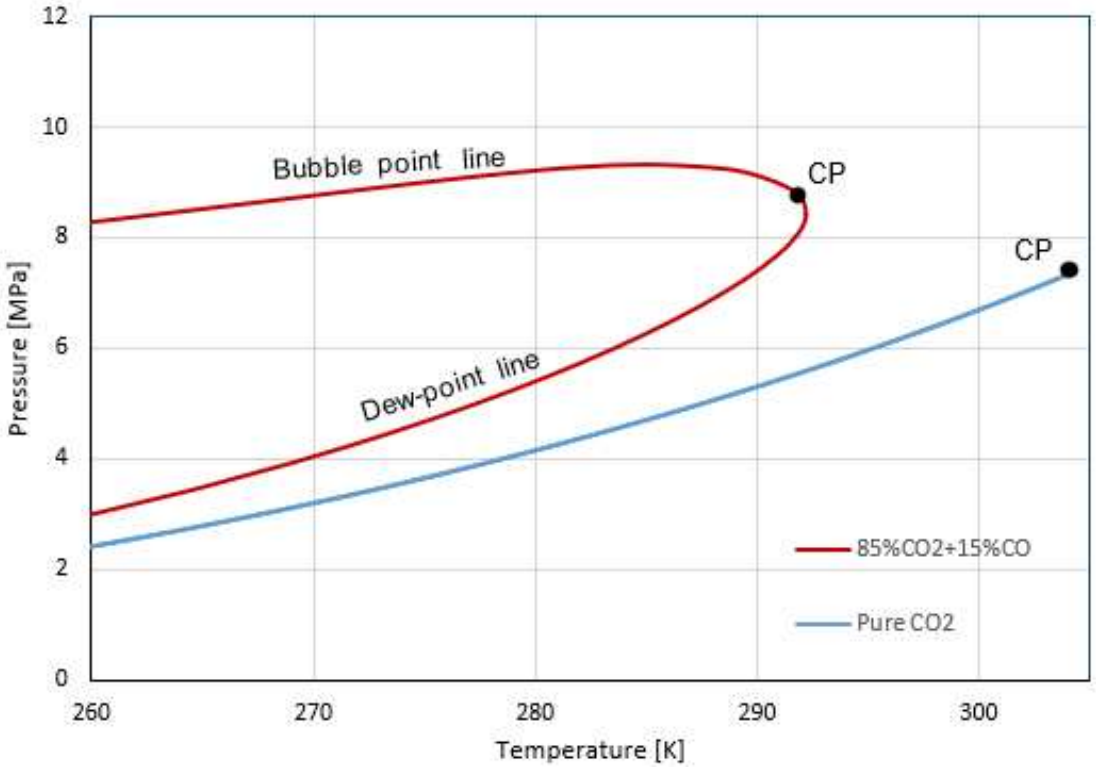

Source: Prepared by the author.

3.1.1 Flash calculation

Flash calculations determine the equilibrium distribution of components between different phases at a given temperature and pressure. These calculations are essential for simulating and optimizing energy industry processes, such as hydrocarbon production and transport (Zhang et al., 2022).

Traditional flash calculation solves equations of state to find equilibrium phase compositions, often relying on iterative methods for convergence. The process typically involves a stability analysis to determine if phase separation will occur, followed by phase split calculations to determine the equilibrium compositions (Liang, 2018).

According to formulation presented by Pedersen; Christensen; Shaikh (2024), the ratio between vapor and liquid-phase mole fraction is termed the equilibrium ratio, or K-factor (K_i). This equilibrium relationship can be expressed using the K-factor, as shown in

$$K_i = \frac{y_i}{x_i} = \frac{\varphi_i^L}{\varphi_i^V} \quad (1)$$

where y_i represents the mole fraction in the gas phase, x_i represents the mole fraction in the liquid phase, vapor and liquid phase fugacity coefficients of component i (φ_i^V and φ_i^L, respectively).

The material balance for each component is given by

$$z_i = \beta y_i + (1 - \beta)x_i \quad (2)$$

where z_i represents the component mole fraction in the feed, and the term β denotes the vapor mole fraction. Consequently, by combining Equations 1 and 2, the relationship of Equations 3 and 4 is created:

$$x_i = \frac{z_i}{1 + \beta(K_i - 1)} \quad (3)$$

$$y_i = \frac{z_i K_i}{1 + \beta(K_i - 1)} \quad (4)$$

Introducing the restriction of $\sum x_i = 1$ and $\sum y_i = 1$ to Equations 3 and 4, and subtracting these restrictions, results in

$$\sum_{i=1}^{N}(y_i - x_i) = \sum_{i=1}^{N} \frac{z_i(K_i - 1)}{1 + \beta(K_i - 1)} = 0 \quad (5)$$

where $F(\beta) = \sum_{i=1}^{N}(y_i - x_i) = 0$, with F as the feed molar flow rate and N the number of the mixture components.

Solving Equation 5 is further complicated by the fact that the fugacity coefficients in Equation 1 are themselves functions of the phase compositions (the very quantities the flash calculation seeks to determine). This interdependence necessitates an iterative solution approach (Figure 6).

Figure 6 – Diagram of the iterative process for flash calculation

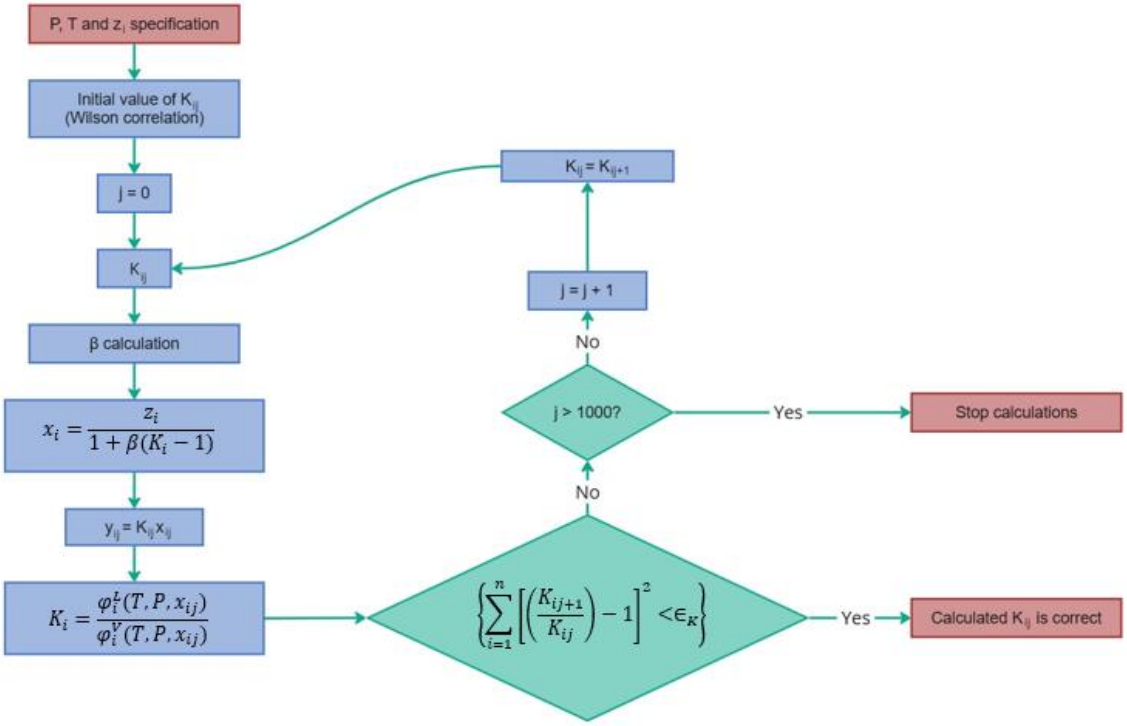

Source: Adapted from Guedes (2023).

3.1.2 Fugacity

Phase equilibrium thermodynamics relies on the concept of fugacity. PEDERSEN; CHRISTENSEN; SHAIKH (2014) shows that the fugacity f is defined through the

$$dG = RT\ d\ln f \tag{6}$$

which for a component i in a mixture can be written as

$$\mu_i = \mu_i^o + RT\ \ln f_i \tag{7}$$

where G is the Gibbs free energy, R the universal gas constant, T the temperature, μ_i the chemical potential and μ_i^o the reference chemical potential of the component i.

For any component i, the fugacity must be identical in all coexisting phases at equilibrium, the fugacity must be the same for all phases existing in equilibrium, therefore $\hat{f}_i^V = \hat{f}_i^L$. The fugacity equation depends on the chosen thermodynamic

model, whether it's based on an EoS (φ/φ) or excess Gibbs free energy (γ/φ). In either case, it can be calculated using φ_i^V and φ_i^L as defined in

$$\hat{f}_i^V = y_i \hat{\varphi}_i^V P \ \therefore \ \hat{f}_i^L = x_i \hat{\varphi}_i^L P \tag{8}$$

where P is the pressure.

3.2 THERMODYNAMIC MODELING

3.2.1 GERG-2008 formulation

This model was developed by a European consortium of natural gas companies (*Groupe Européen de Recherches Gazières* – GERG) dedicated to research and development of technologies for the gas industry, whose objective was to develop an equation of state that would be considered an ISO (International Organization for Standardization) standard for modeling natural gases, ISO 20765-2 (*About Us - GERG*, n.d.).

According to Kunz and Wagner (2012), GERG-2008 is an improved version of GERG-2004, which arose from the need for a new model that aimed to improve the accuracy of thermodynamic properties, which would meet various applications involving natural gases, and mainly, to expand the range of validity to the entire fluid region, criteria that the existing models (Peng-Robinson and AGA8-DC92, for example) did not meet until then. The main difference between the two models is that the new model now covers 21 components, while its previous version covered only 18. Besides that, the amount of experimental data considered in the adjust process also was updated.

This equation of state is described in the explicit form of the Helmholtz free Energy (a) with the independent variables being density (ρ), temperature (T) and molar composition ($\bar{x}$), as shown in

$$a(\rho, T, \bar{x}) = a^o(\rho, T, \bar{x}) + a^r(\rho, T, \bar{x}) \tag{9}$$

The function $a(\rho, T)$ comprises the part that describes the properties of the ideal gas (a^o), and the part that describes the residual behavior of the mixture

(a^r). Equation 9 can also be written in its dimensionless form (Equation 10), described by the reduced density (δ) and the inverse of the reduced temperature (τ), dependent on the critical density (ρ_c) and critical temperature (T_c) with $\delta = \rho/\rho_c$ and $\tau = T_c/T$ where $\rho_c = \rho_r(\bar{x})$ and $T_c = T_r(\bar{x})$, and for Equations 11 and 12.

$$\alpha(\delta, \tau, \bar{x}) = \alpha^o(\delta, \tau, \bar{x}) + \alpha^r(\delta, \tau, \bar{x}) \tag{10}$$

$$\alpha^0(\rho, T, \bar{x}) = \sum_{i=1}^{N} x_i[\alpha_{oi}^o(\rho, T) + \ln x_i] \tag{11}$$

$$\alpha^r(\delta.\tau, \bar{x}) = \sum_{i=1}^{N} x_i \alpha_{oi}^r(\delta, \tau) + \Delta\alpha^r(\delta, \tau, \bar{x}) \tag{12}$$

In the Equations 11 and 12, N is the number of components in the mixture, α_{oi}^o is the dimensionless form of the Helmholtz free energy in the ideal gas state of component i, the terms $x_i \ln x_i$ refers to the entropy of the mixture, α_{oi}^r is the residual part of the reduce Helmholtz free energy of component i, and $\Delta\alpha^r$ is the departure function defined by

$$\Delta\alpha^r(\delta, \tau, \bar{x}) = x_i x_j F_{ij} \alpha_{ij}^r(\delta, \tau). \tag{13}$$

The term F_{ij} is considered 1 for binary specific departure functions, tuned for binary generalized departure function, and considered zero for departure functions that were not developed by GERG-2008.

The dimensionless form of the Helmholtz free energy in the ideal gas state of component i in Equation 11 is given by Equation 14, where $R^* = 8.314510 J \cdot mol^{-1} \cdot K^{-1}$ and $R = 8.314472 J \cdot mol^{-1} \cdot K^{-1}$. The coefficients $n_{oi,k}^o$ and $\vartheta_{oi,k}^o$ are in Table A1 of the article by Kunz and Wagner (2012) and are specific to each of the 21 components.

$$\alpha_{oi}^{o}(\rho,T)=\ln\left(\frac{\rho}{\rho_{c,i}}\right)+\frac{R^{*}}{R}[n_{oi,1}^{o}+n_{oi,2}^{o}\frac{T_{c,i}}{T}+n_{oi,3}^{o}\ln\left(\frac{T_{c,i}}{T}\right)+\sum_{k=4,6}n_{oi,k}^{o}\ln\left(\left|\sinh\left(\vartheta_{oi,k}^{o}\frac{T_{c,i}}{T}\right)\right|\right)-\sum_{k=5,7}n_{oi,k}^{o}\ln\left(\left|\cosh\left(\vartheta_{oi,k}^{o}\frac{T_{c,i}}{T}\right)\right|\right)] \quad (14)$$

The residual part of the reduced Helmholtz free energy of component i in Equation 12 is defined by Equation 15 and the parameters $n_{oi,k}$, $d_{oi,k}$, $t_{oi,k}$ and $c_{oi,k}$ have also been defined and listed in Table A2 – A4 of Kunz and Wagner (2012) article for each of the components considered.

$$\alpha_{oi}^{r}(\delta,\tau)=\sum_{k=i}^{K_{Pol,i}}n_{oi,k}\delta^{d_{oi,k}}\tau^{t_{oi,k}}+\sum_{k=K_{Pol,i}+1}^{K_{Pol,i}+K_{Exp,i}}n_{oi,k}\delta^{d_{oi,k}}\tau^{t_{oi,k}}e^{-\delta^{c_{oi,k}}} \quad (15)$$

The departure function aims to further improve the accuracy of the multifluid mixture model in describing thermodynamic properties when the adjustment of the reduction function parameters with accurate experimental data is not sufficient. In general, this term has a smaller contribution to the residual behavior of the mixture than α_{oi}^{r}. Equation 16 describes the function $\alpha_{ij}^{r}(\delta,\tau)$ present in Equation 13, where the values of $n_{ij,k}$, $d_{ij,k}$, $t_{ij,k}$, $\eta_{ij,k}$, $\varepsilon_{ij,k}$, $\beta_{ij,k}$ and $\gamma_{ij,k}$ are also available in Kunz and Wagner (2012) article in Table A7.

$$\alpha_{ij}^{r}(\delta,\tau)=\sum_{k=1}^{K_{Pol,ij}}n_{ij,k}\delta^{d_{ij,k}}\tau^{t_{ij,k}}+\sum_{k=K_{Pol,ij}+1}^{K_{Pol,ij}+K_{Exp,ij}}n_{ij,k}\delta^{d_{ij,k}}\tau^{t_{ij,k}}\cdot\exp[-\eta_{ij,k}(\delta-\varepsilon_{ij,k})^{2}-\beta_{ij,k}(\delta-\gamma_{ij,k})] \quad (16)$$

Finally, the variable δ and τ are determined by Equations 17 and 18, respectively. Furthermore, the relationship between the terms γ and β for volume v and temperature (T) are presented in Equation 19.

$$\frac{1}{\rho_r(\bar{x})} = \sum_{i=1}^{N} x_i^2 \frac{1}{\rho_{c,i}} + \sum_{i=1}^{N-1} \sum_{j=i+1}^{N} 2x_i x_j \beta_{v,ij} \gamma_{v,ij} \frac{x_i + x_j}{\beta_{v,ij}^2 x_i + x_j} \frac{1}{8} \left(\frac{1}{\rho_{c,i}^{1/3}} + \frac{1}{\rho_{c,j}^{1/3}} \right)^3 \quad (17)$$

$$T_r(\bar{x}) = \sum_{i=1}^{N} x_i^2 T_{c,i} + \sum_{i=1}^{N-1} \sum_{j=i+1}^{N} 2x_i x_j \beta_{T,ij} \gamma_{T,ij} \frac{x_i + x_j}{\beta_{T,ij}^2 x_i + x_j} \left(T_{c,i} \cdot T_{c,j} \right)^{0.5} \quad (18)$$

$$\gamma_{v,ij} = \gamma_{v,ji},\ \gamma_{T,ij} = \gamma_{T,ji} \text{ and } \beta_{v,ij} = \frac{1}{\beta_{v,ji}},\ \beta_{T,ij} = \frac{1}{\beta_{T,ji}} \quad (19)$$

The parameters $\gamma_{v,ij}$, $\gamma_{T,ij}$, $\beta_{v,ij}$ and $\beta_{T,ij}$, as well as F_{ij}, are adjustable terms based on the experimental data available for each of the mixtures. Figure 7 shows an overview of the 210 binary combinations resulting from the 21 natural gases considered in the development of GERG-2008 and illustrates the different types of functions used in the description of binary mixtures.

Figure 7 – Binary interactions in GERG-2008

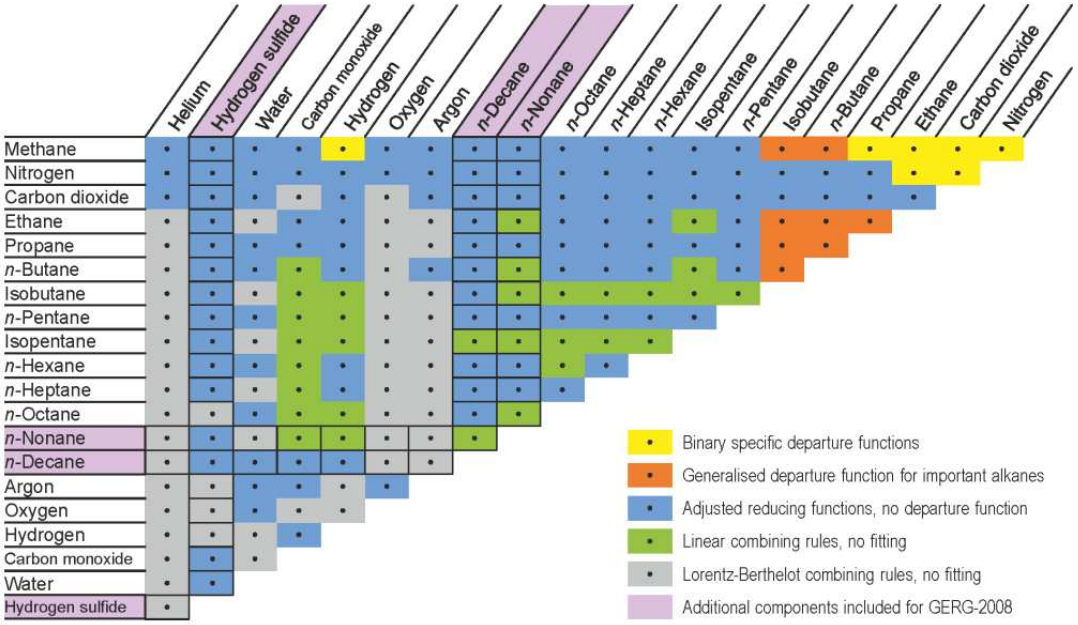

Source: Kunz and Wagner (2012).

GERG-2008 covers the entire composition range of mixture (0% - 100%) very well and presents two validation range for $90K \leq T \leq 450K$ and pressures up to 35MPa, and the extended range for $60K \leq T \leq 700K$ and pressures up to 70MPa.

3.2.2 EOS-CG 2019 formulation

GERG-2008 was developed for natural gases with impurities, while EOS-CG (Equation of State for Combustion Gases and Combustion Gas like Mixture) was developed for combustion gases, with CO_2 as the main component. The first version of the EOS-CG model from 2013, presented by Gernert (2013) and Gernert and Span (2016), uses the same mathematical approach as GERG-2008, with small adjustments to improve the description of binary mixtures of 6 substances already addressed by GERG-2008. These adjustments aim to increase the precision of the phase transition region for a wider range of pressure and temperature for CO_2 mixtures and the solubility of gases in water, points where GERG-2008 had limitations.

A more recent version of EOS-CG was developed by HERRIG (2018) in 2019, with the aim of expanding the number of substances considered from 6 to 14, commonly found in CO_2-rich mixtures, in addition to developing an EoS for heavy water. This development relied on the use of new experimental data.

While GERG-2008 used a simplified version of the pure fluid reference equation for Helmholtz free energy, EOS-CG 2019 uses the pure fluid reference equation specific to each substance considered (Table 2), which ensures better performance. EOS-CG 2013 also followed this approach, but Herring (2018)'s version applied improvements to some of the existing models.

Table 2 – Helmholtz equations of state used for the pure components in the EOS-CG 2019 mixture model.

Component	Pure fluid equation used in the EOS-CG 2019 mixture model
Carbon dioxide	Reference EoS by Span and Wagner (1996b)
Water	Reference EoS by Wagner and Pruss (2002)
Nitrogen	Reference EoS by Span Et Al. (2000)
Oxygen	Reference EoS by Schmidt and Wagner (1985)
Argon	Reference EoS by Tegeler; Span; Wagner (1999)
Carbon monoxide	Short industrial EoS by Lemmon and Span (2006)
Hydrogen	Reference EoS by Leachman et al. (2009)
Methane	Reference EoS by Setzmann and Wagner (1991)

Component	Pure fluid equation used in the EOS-CG 2019 mixture model
Hydrogen sulfide	Short industrial EoS of Lemmon and Span (2006)
Sulfur dioxide	EoS of Gao et al. (2016)
Monoethanolamine	EoS developed in Herrig (2018)
Diethanolamine	EoS of Kortmann (2016)
Chlorine	EoS developed in Herrig, 2018
Hydrogen chloride	EoS of Thol et el. (2018)

Source: adapted by HERRIG (2018).

As mentioned previously, EOS-CG 2019 uses the same equations as GERG-2008 (Equations 9 through 19, with two notable exception: Equation 14 is replaced by the models presented in Table 2, and Equation 16. The latter equation, referring to the term $\alpha_{ij}^{r}(\delta,\tau)$, is replaced by the one presented in Equation 20 in a general form, encompassing all possible types of terms. The selection of the type and number of terms is determined by the correlator during the fitting of EoS to the thermodynamic property data of the specific binary mixture.

$$\begin{aligned}\alpha_{ij}^{r}(\delta,\tau) = &\sum_{k=1}^{K_{Pol,ij}} n_{ij,k}\delta^{d_{ij,k}}\tau^{t_{ij,k}} \\ &+ \sum_{k=K_{Pol,ij}+1}^{K_{Pol,ij}+K_{Exp,ij}} n_{ij,k}\delta^{d_{ij,k}}\tau^{t_{ij,k}}\exp\left(-\delta^{l_{ij,k}}\right) \\ &+ \sum_{k=K_{Pol,ij}+K_{Exp,ij}+1}^{K_{Pol,ij}+K_{Exp,ij}+K_{spec,ij}} n_{ij,k}\delta^{d_{ij,k}}\tau^{t_{ij,k}}\exp\left[-\eta_{ij,k}\left(\delta-\varepsilon_{ij,k}\right)^{2}\right. \\ &\left.-\beta_{ij,k}\left(\delta-\gamma_{ij,k}\right)\right] \\ &+ \sum_{k=K_{Pol,ij}+K_{Exp,ij}+K_{spec,ij}+1}^{K_{Pol,ij}+K_{Exp,ij}+K_{spec,ij}+K_{GBS,ij}} n_{ij,k}\delta^{d_{ij,k}}\tau^{t_{ij,k}}\exp\left[-\eta_{ij,k}\left(\delta\right.\right. \\ &\left.\left.-\varepsilon_{ij,k}\right)^{2}-\beta_{ij,k}\left(\tau-\gamma_{ij,k}\right)^{2}\right]\end{aligned} \qquad (20)$$

Figure 8 provides an overview of the binary mixtures involving the 14 substances considered in this study. The components are classified as major or minor, based on their mole fraction in typical CCS mixtures. It is important to note

that carbon monoxide, hydrogen, and methane can occur as major or minor components, depending on the design of the CCS process.

Figure 8 – Binary interactions in EOS-CG 2019

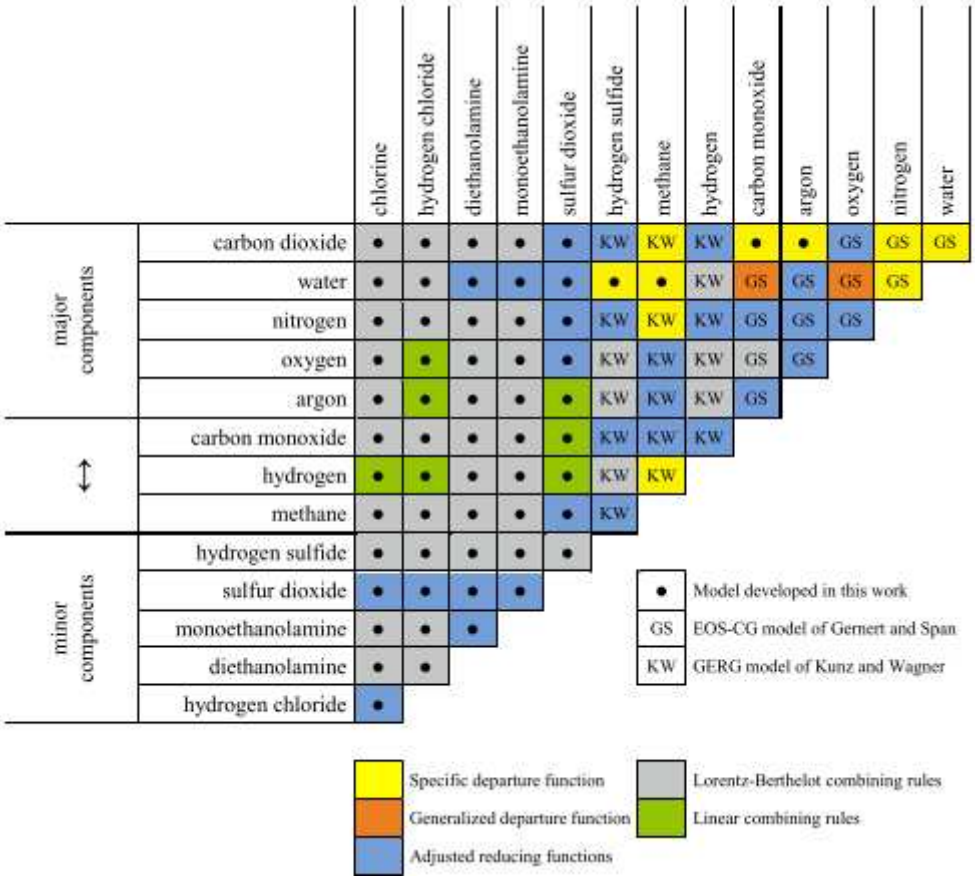

Source: Herrig (2018)

In terms of applicability, the multicomponent mixture model in question is valid in the entire stable fluid region (62 K ≤ T ≤ 2000 K and p ≤ 800 MPa). However, it is crucial to note that solid states of water and CO_2, as well as hydrates, are not considered in this model.

3.3 DATA COLLECTION

Data collection occurred exclusively from reliable literary sources, including scientific article, theses, and dissertations. The research sought studied presenting experimental density measurements performed under controlled temperature and pressure conditions for $CO_2 + CO$, $CO_2 + Ar$ and $CO_2 + CH_4$

mixtures. Furthermore, the selected studies explicitly reported the experimental errors associated with the measurements.

The collected experimental data underwent tabulation and organization according to the studies gas combinations and their concentrations. To ensure consistency, the research converted the data to standard units of density (kg/m^3), pressure (MPa) and temperature (K), when necessary. Subsequently, the research performed an analysis for outlier identification applying the Local Outlier Factor method. The research disregarded data presenting as outliers, meaning outside the expected range, to avoid data pollution in subsequent analyses.

The selected data were organized into a spreadsheet in Microsoft Excel, where each reference received an identification code (ID) for easy detection of the original data sources. The references used are presented in Table 3.

Table 3 – References of analyzed experimental data.

Mixture	Author	Year	Num. of data	Impurity mole fraction range	Temperature range [K]	Pressure range [MPa]
$CO_2 + CO$	SOUZA et al.	2019	219	0.01-0.50	283.15-373.15	1.90-31.98
$CO_2 + CO$	BLANCO et al.	2014	1151	0.004-0.03	253.15-353.15	0.094-20.2
$CO_2 + Ar$	YANG et al.	2015	39	0.95-0.99	298.22-398.36	14.97-4.97
$CO_2 + Ar$	TSANKOVA et al.	2017	58	0.05-0.25	260.14-313.30	0.45-7.08
$CO_2 + Ar$	BEN SOUISSI et al.	2017	56	0.25-0.50	273.15-323.15	0.50-9.05
$CO_2 + Ar$	MANTOVANI et al.	2012	103	0.03-0.17	302.22-383.14	1.00-19.0
$CO_2 + Ar$	KESTIN; KOBAYASHI; WOOD	1966	23	0.08-0.36	293.15-303.15	0.10-2.57
$CO_2 + Ar$	WEGGE	2016	211	0.25-0.50	253.15-353.15	0.99-20.0
$CO_2 + CH_4$	ARAI; KAMINISHI; SAITO	1971	145	0.0006-0.58	273.15-301.15	2.42-45.11
$CO_2 + CH_4$	AL-SIYABI	2013	33	0.001-0.025	283 .15-301.15	6.64-44.55

Source: Prepared by the author.

In summary, approximately 2040 experimental densities data were collected, most of which were to the $CO_2 + CO$ mixture. It is worth noting that most of the references considered here were published after GERG-2008 and therefore are not considered in its development. Table 4 synthesize the general information from this collection for each of the systems considered.

Table 4 – Summary of experimental density data considered for each of the mixture studied.

Mixture	Num. of data	Impurity mole fraction range	Temperature range [K]	Pressure range [MPa]
$CO_2 + CO$	1370	0.004-0.50	253.15-373.15	0.094-31.98
$CO_2 + Ar$	490	0.03-0.99	253.15-398.36	0.10-45.11
$CO_2 + CH_4$	178	0.0006-0.58	273.15-301.15	2.22-45.11

Source: Prepared by the author.

3.4 SIMULATIONS IN MULTIFLASH

3.4.1 Data preprocessing

The data points are encompassed in datasets for each CO2—Impurity binary system. For each impurity dataset, a two-fold cross validation is adopted, randomly splitting the data. These are referred to as dataset 1 and dataset 2 in this study (see Figure 9 for an illustration of this procedure). Each data fold is then randomly divided as a training set (75% of the data) and a validation set (25% of the data). These stratifications allow a fair study of model calibrations by using the validation data to check the model predictive capability since only the training data are used to fit the model parameters in the analyses performed in this work.

Figure 9 – Illustration of dataset splitting into training and validation set.

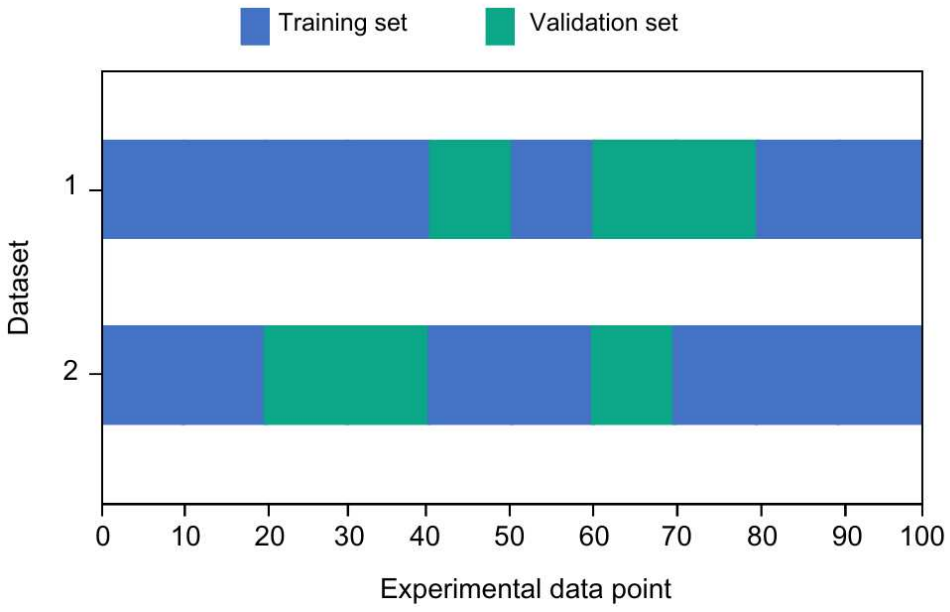

Source: Prepared by the author.

Moreover, the Multiflash Excel application programming interface (API) classified the data by phase within each stratification. Points identified by API as two-phase were discarded to prevent potential outliers, as the simulated data represent single-phase densities only.

3.4.2 Tuning of the models

Models tuning was performed using the Multiflash Thermobuilder tool. This involved creating multiple base case files for each impurity and each studied model (GERG-2008 and EOS-CG 2019). These base cases provided the necessary information about the mixture components and the model to the software.

Thermobuilder also utilized base files for each impurity and dataset. These files were generated by uploading the training set into the segmented tables in the software graphical user interface. Each input table was based on data reference, phase and impurity mole fraction.

The subsequent step involved adjusting each model. This included testing various combinations of fitting parameters and evaluating the objective function values and errors between the experimental densities and the densities simulated from these adjustments. The tested combinations are presented in Table 5.

Table 5 – Investigated combinations of tuning parameters.

Combination ID	Tuning parameters
1	$\beta_{T,ij}$ and $\gamma_{T,ij}$
2	$\beta_{v,ij}$ and $\gamma_{v,ij}$
3	F_{ij}
4	$\beta_{T,ij}$, $\gamma_{T,ij}$, $\beta_{v,ij}$ and $\gamma_{v,ij}$
5	$\beta_{T,ij}$, $\gamma_{T,ij}$ and F_{ij}
6	$\beta_{v,ij}$, $\gamma_{v,ij}$ and F_{ij}
7	$\beta_{T,ij}$, $\gamma_{T,ij}$, $\beta_{v,ij}$, $\gamma_{v,ij}$ and F_{ij}

Source: Prepared by the author.

All simulation results were tabulated, paired with the corresponding experimental data, and subsequently compared. The fitting parameters values

and combination yielding model outputs with the best performance for the training set were selected. This calibrated model was then applied to the selected validation set (using the Multiflash Excel API), and the resulting densities were compared with experimental densities, with the Root Mean Square Error (RMSE), Mean Absolute Error (MAE), and Absolute Relative Error (ARE) values calculated (further details on statistical metrics are provided in Section 3.3). For comparison's sake, the model parametrized with the Multiflash's default values are evaluated with the same experimental dataset and statistical metrics. This comparison assesses the tuning effectiveness in density prediction compared to the original model.

As a final validation, this tuned model was applied to the complete impurity dataset (training and validation), and error analysis, segmented by impurity mole fractions, was performed (for both original and tuned models). Additionally, critical points were simulated for 3%, 5%, 15% and 25% impurity levels, aiming to identify the impact of the adjustment on this determination.

To compare the overall results obtained from the fitting of the equations of state, for each impurity and EoS, only the calibrated model that best performed with the validation set was selected. The main results found previously were summarized through tables to facilitate analysis and determination of which model is the most efficient.

3.4.3 Phase envelopes

The phase envelope generation comprised the selection of impurity fractions representative of CO_2 capture processes (3%, and 5%) and molar fraction higher, as 15% and 25%. The process employed Multiflash and applied the best equation of state for each system (model tuning section) to generate comparative phase envelopes for mixture across different concentrations.

A further analysis was conducted to examine the effect of the three impurities (CO, Ar and CH_4), each maintained at a 5% molar fraction, under identical conditions. The results are presented in a single figure. Both analyses included a simulation of the pure CO_2 phase envelope to aid in understanding the impact of impurities on CO_2-rich mixtures. The pure CO_2 simulation used

Multiflash "CO_2 high-accuracy model", based on model of Span and Wagner (1996).

3.4.4 Densities

Density behavior analyses employed the same equations of states and molar fractions discussed in the previous section for each impurity. The pressure and temperature ranges for the density simulations were chosen based on the validity limits of the respective equations of state.

The densities calculation was done using Multiflash Excel API, considering the density estimates for three temperatures: 273.15 K (where a two-phase region may exist, depending on the pressure), 300.15 K (a temperature close to the critical points), and 353.15.K (at which the system is in the supercritical region, depending on the pressure and it is an operation temperature of CO_2 geological storage). To provide a basis for comparison, pure CO_2 under the same conditions using the Span-Wagner equation of state was also simulated.

The results appear as graphs to aid in visualizing the impact of impurities on density behavior across various pressure and temperature conditions.

3.5 STATISTICAL ANALYZES

To determine which model best fits the system, this work compares the density values simulated for each Equation of State (EoS) with experimental values form the literature. This comparison used the Root Mean Square Error (RMSE), Mean Absolute Error (MAE), and Absolute Relative Error (ARE) metrics, defined by Equations 21-23, respectively. In these equations, n represents the number of data points analyzed for a given scenario, y_i denotes the experimental density values, and $\hat{y}_i$ represents the values predicted by the models (simulated densities).

$$RMSE = \sqrt{\frac{1}{n}\sum_{i=1}^{n}(y_i - \hat{y}_i)^2} \tag{21}$$

$$MAE = \frac{100}{n}\sum_{i=1}^{n}|y_i - \hat{y}_i| \quad (22)$$

$$ARE = \left|\frac{y_i - \hat{y}_i}{y_i}\right| \cdot 100 \quad (23)$$

Both indicators are widely used for evaluating the accuracy of prediction models and for measuring how much simulated data deviates from experimental data. RMSE and MAE uses the same unit as the studied property, whereas ARE use percentages.

4 RESULTS AND DISCUSSIONS

This section is divided into three main steps: (1) comparison between the tuning of the models described in Appendices A, B and C, (2) analyzing the impact of impurities on the phase envelope and (3) the densities. Figure 10 shows the flowchart of the processes followed to obtain the results, as well as the classification of the data used.

In the first part, the adjustable parameters of GERG-2008 and EOS-CG 2019 models were fine-tuned for which combinations of the Table 5 using experimental densities for mixtures of $CO_2 + CO$, $CO_2 + Ar$ and $CO_2 + CH_4$ mixtures. The quality of the tune was validated by analyzing the statistical errors. The evaluation of the models for different impurity mole fractions on critical point predictions are also considered.

In the next step, comparison was made between the tunes of each of the models and their original version, based on the statistical error values, with the aim of identifying the best model for each mixture and then defining the validity range for this model. Finally, applying the best model identified for each mixture as being the most suitable for predicting densities, was analyzed the impact of the presence of impurities on the phase behavior and, subsequently, on the density, comparing the results with the case of pure CO_2.

Figure 11 is a visual representation of Table 5, which shows the parameters that have been adjusted in each of the combinations. These arrangements were made in such a way as to cover all the possible combinations between the β_T, γ_T, β_v, γ_v and F_{ij} parameters, making it easy to identify the influence of each parameter on the model's tune.

Figure 10 – Step by step flowchart of results

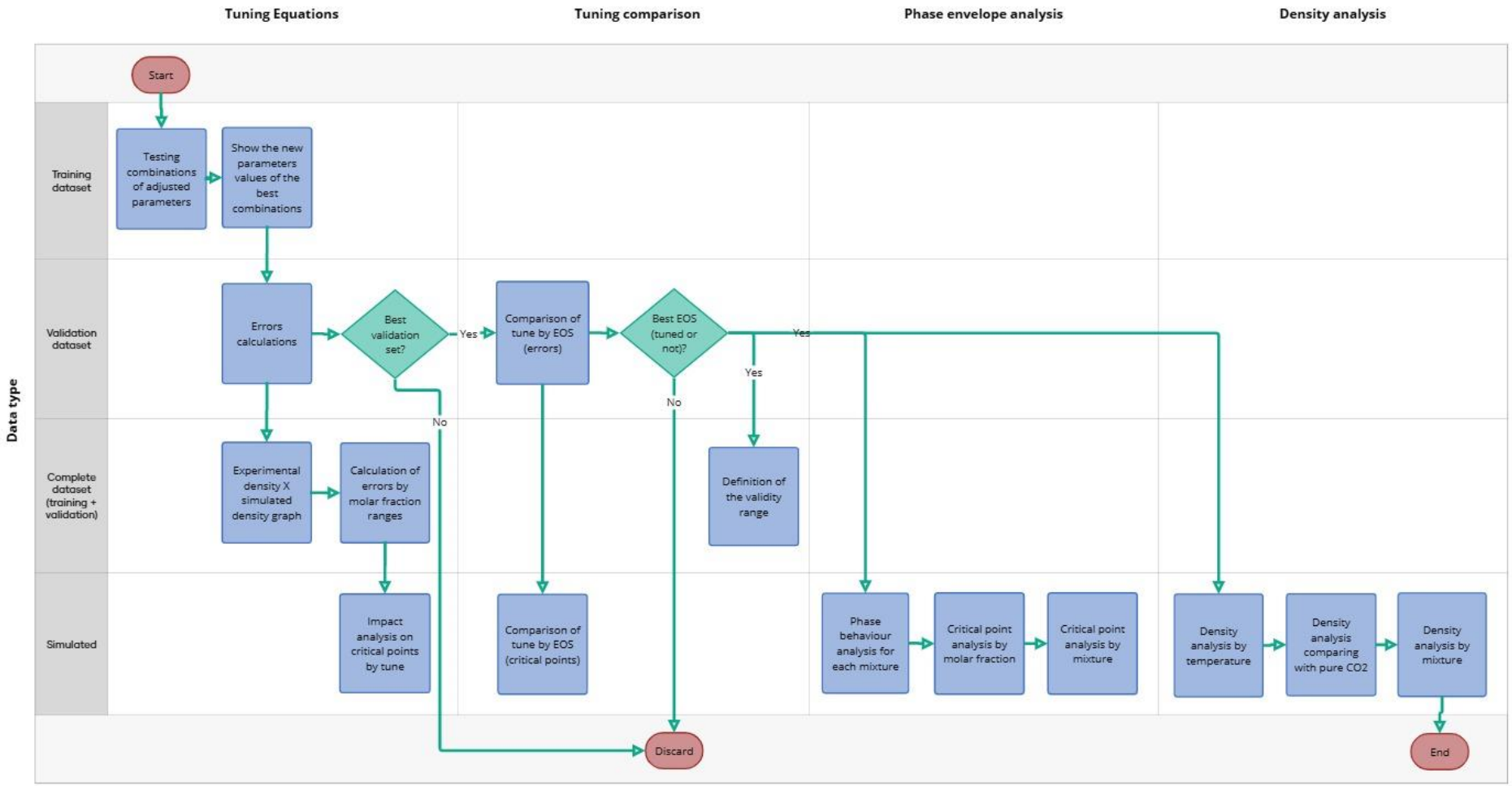

Source: Prepared by the author.

Figure 11 – Tuned parameters in each combination

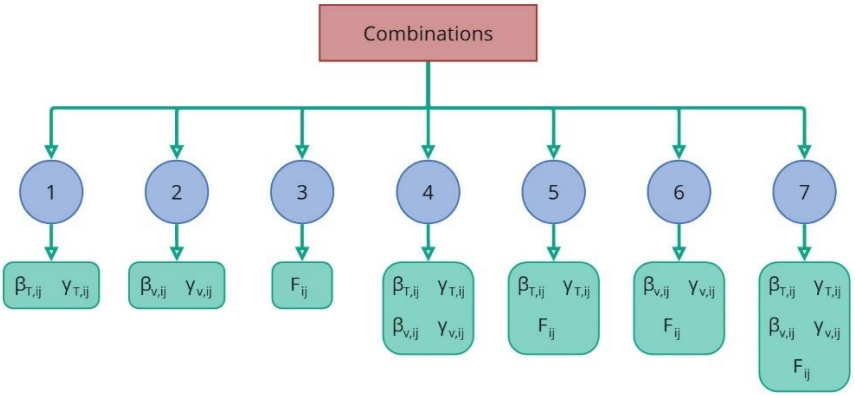

Source: Prepared by the author.

4.1 COMPARISON OF FITTING RESULTS

The tuning process with the main results has been detailed in Appendices A, B and C for impurities CO, Ar, CH_4, respectively, for both the GERG-2008 model and the EOS-CG 2019. The results have been summarized and can be observed in Figure 12.

Figure 12 – Synthesis of tune results analyses

	CO2+CO		CO2+Ar		CO2+CH4	
	GERG-2008	EOS-CG 2019	GERG-2008	EOS-CG 2019	GERG-2008	EOS-CG 2019
Original parameters	$\beta = \gamma = 1$ $F_{ij} = 0$	β and γ tuned $F_{ij} = 1$	β and γ tuned $F_{ij} = 1$	β and γ tuned $F_{ij} = 1$	β and γ tuned $F_{ij} = 1$	Same as GERG-2009
Does the Fij tune influence the result?	✗	✗	✓	✓	✗	✓
Adjustable parameters most influential in tuning	Related to Temperature	Related to Volume	Related to Temperature	Related to Temperature	Related to Temperature	
Best combination	4	Dataset 1: 3 Dataset 2: 4	7	5	1	6
Was the tune effective?	✓	✗	✓	✓	✓	✓

Source: Prepared by the author.

In the $CO_2 + CO$ system, the adjusted GERG-2008 showed an improvement compared to its original form, with slightly larger errors than the original EOS-CG 2019. Adjusting the EOS-CG 2019 did not improve the model performance, indicating that its original version is more suitable for predicting the system density. For GERG-2008, the range of 3% to 5% CO, among the ranges

evaluated, was the one that presented the greatest impact of the adjustment, considerably reducing the error values. For EOS-CG 2019, this range was also the one that presented the smallest statistical errors.

For the case of the Ar as an impurity, both adjusted models showed improvements in error values, and as expected, the EOS-CG 2019 delivered better results than the adjusted GERG-2008, making it more suitable for this mixture. For EOS-CG 2019, in range of interest of 3% to 5%, it had a greater impact on the reduction of ARE when compared to the GERG-2008 tune.

Regarding the $CO_2 + CH_4$ system, both adjusted models demonstrated improved performance compared to their respective original models, with the tuned GERG-2008 yielding even better results than the tuned EOS-CG 2019. A key observation from the preceding results is that, despite the original models for the $CO_2 + CH_4$ system utilizing the same adjustable parameter values, the tuning process resulted in a greater improvement for the GERG-2008 model.

Table 6 comprises the results of the best validation datasets found in the previous session, based on statistical errors, for each equation of state.

The adjustments made to both models led to a more significant improvement for the $CO_2 + CH_4$ system. The adjust model performed better for the system with CH_4 impurity than with CO, reversing the trend observed with the original models, as seen in Table 6.

Table 6 – Summary of model and tuning performance for validation set. The best results are highlighted in bold. Calculated errors based on density values.

Error	GERG-2008		EOS-CG 2019	
	Before	After	Before	After
		$CO_2 + CO$ (340 data)		
ARE	3.161	2.919	**2.882**	2.886
MAE	9.597	8.554	**8.492**	8.499
RMSE	24.860	24.738	**24.734**	24.733
		$CO_2 + Ar$ (121 data)		
ARE	1.292	0.764	0.632	**0.520**
MAE	6.706	3.398	2.552	**1.709**
RMSE	13.168	7.005	5.817	**4.329**
		$CO_2 + CH_4$ (36 data)		
ARE	3.985	**2.806**	4.010	2.947
MAE	22.835	**17.784**	22.934	18.056
RMSE	34.148	**28.667**	34.217	28.694

Source: Prepared by the author.

In general, for the case of CO_2 with CO as an impurity, the original EOS-CG 2019 still appears to be the best option, since its error values are better than the adjusted GERG-2008. With the presence of argon, the tuned EOS-CG 2019 better fits the results. And finally, for CH_4, the tuned GERG-2008 was shown to be better than both the original and tuned EOS-CG 2019.

Based on the experimental data used to tune the models, Table 7 shows the validation range for each model. It is worth noting that for $CO_2 + CO$, this range refers to the original EOS-CG 2019 model provided by HERRIG (2018), as it proved to be more suitable for this system than the other proposed models.

Table 7 – Model validity ranges by mixture.

Mixture	Impurity molar fraction range	Temperature range [K]	Pressure range [MPa]
$CO_2 + CO$	0.004 – 0.75	253 – 423	p < 50 MPa
$CO_2 + Ar$	0.03 – 0.99	253.15 – 398.15	0.10 – 24.97
$CO_2 + CH_4$	0.0006 – 0.58	273.15 – 301.15	2.42 – 45.11

Source: Prepared by the author.

Figure 13 summarize the ranking of the models studied in terms of their capacity to predict densities. In the next section, for each mixture analyzed, the best model was used to evaluate the impact of impurities on some thermodynamic properties. It should be remembered that the models used in this study were not tuned based on experimental phase equilibrium data, only density data.

Figure 13 – Ranking of the EoS selection that presented the best error values for validation data for each mixture.

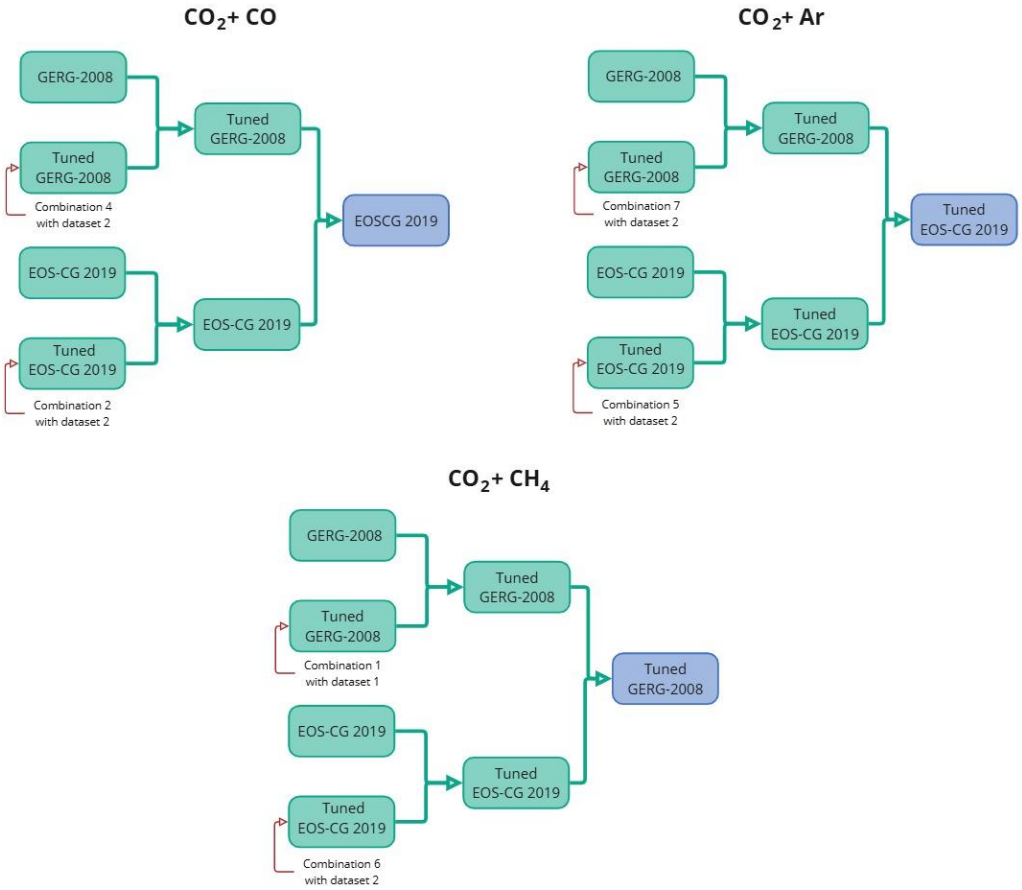

Source: Prepared by the author.

4.2 INFLUENCE OF IMPURITIES ON DENSITY AND PHASE ENVELOPE

This session will analyze the impact of impurities, using the EoS defined above, on the description of densities and phase envelopes. These analyses were carried out separately for each mixture in order to verify the influence of the impurity concentration and, subsequently, a comparison between the impurities (same conditions) to understand which of them would have the greatest impact on the properties studied.

4.2.1 Effect of impurities on density

For the density evaluations, simulations were performed for the three mixture at the same concentrations considered previously, with three fixed temperatures: 273.15 K, 300.15 K and 353.15.K.

From Figure 14 to Figure 16 illustrates the density behavior of the $CO_2 + CO$ mixture at different temperatures. As expected, temperature and density demonstrate an inverse relationship, independent of CO molar fraction. The figures also shows that the presence of higher impurity concentrations results in a reduction of the mixture density.

Figure 14 – Density behavior for the $CO_2 + CO$ mixture at 273.15 K.

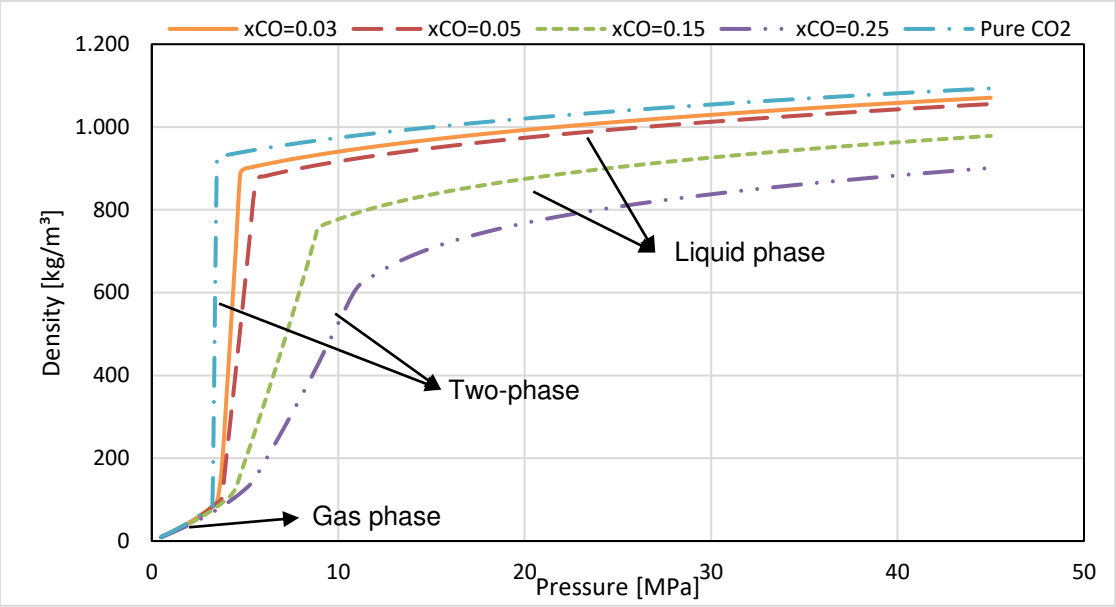

Source: Prepared by the author.

Figure 15 – Density behavior for the $CO_2 + CO$ mixture at 300.15 K.

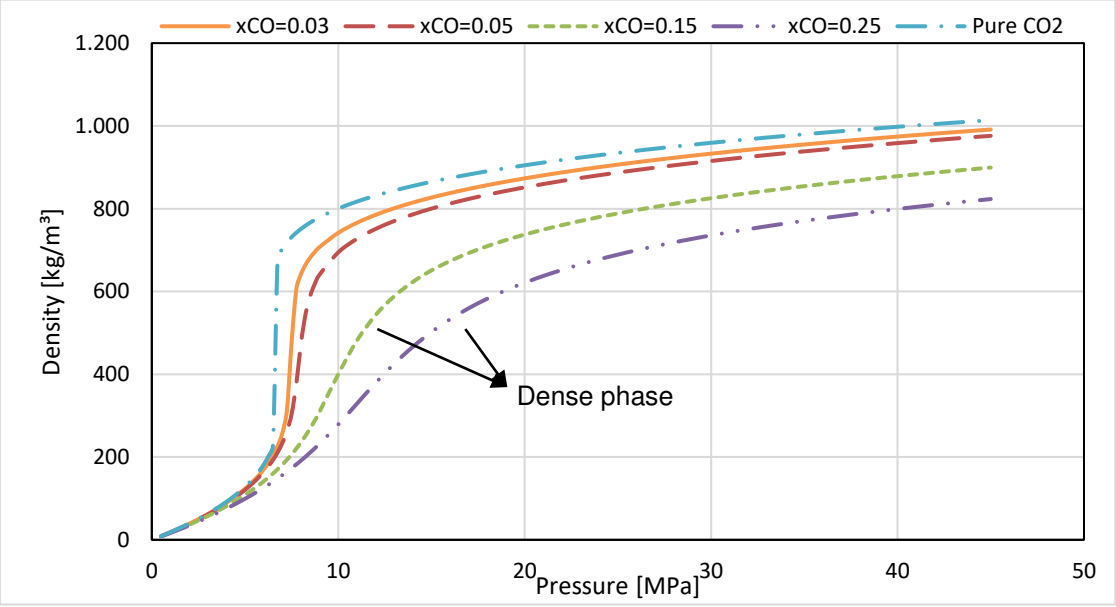

Source: Prepared by the author.

Figure 16 – Density behavior for the $CO_2 + CO$ mixture at 353.15 K.

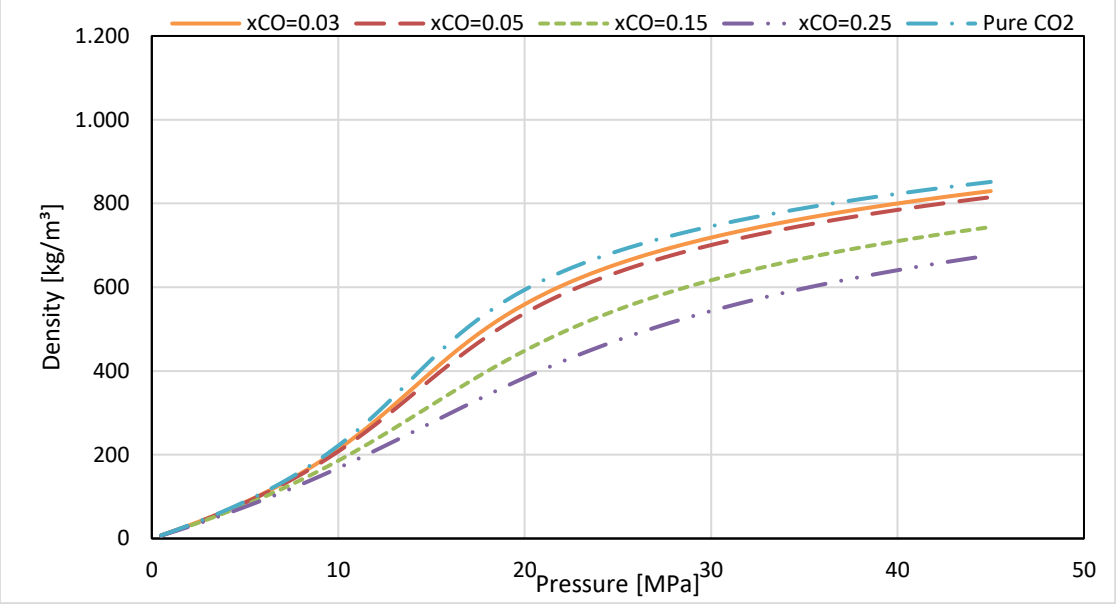

Source: Prepared by the author.

Figure 14 - Figure 15 clarifies the density behavior in each phase of the mixture. While the gas phase shows only minor density variations with changes in concentration and temperature, the two-phase region reveals more pronounced differences among the analyzed cases.

Table 8 summarizes MAE values between pure CO_2 and $CO_2 + CO$ mixture densities at 300.15 K. This temperature was selected due to be near the critical temperatures and can be a sensitive region. This way, it is possible to verify the impact of the impurity compared to the case of pure CO_2.

Table 8 – MAE values (kg/m^3) comparing the density of pure CO_2 with the densities of mixtures containing CO at 300.15 K for phase.

CO molar fraction	Gas phase	Liquid phase	Dense phase
0.03	4.257	52.822	-
0.05	6.575	75.558	-
0.15	166.978	-	164.762
0.25	196.056	-	261.975

Source: Prepared by the author.

For concentrations of 3% and 5% CO, it was observed that the liquid phase had a greater variation in density (pure CO_2 versus $CO_2 + CO$) when compared to the gas phase. This indicates that the effect of the impurity is greater for the liquid

phase at these concentrations. For higher molar fraction, the deviation is considerably higher, as expected. In the case of 15%CO, the MAE values were very similar for the gas phase and the dense phase, while for 25% the impurity was higher. The most significant impact of impurities is in the two-phase region, since pure CO_2 does not exhibit this region and de comparison is not possible, so not included in Table 8.

At lower impurities molar fractions, the gas phase demonstrates the least deviation from pure CO_2 behavior. However, at 15%CO, the MAE values for both gas and dense phase are similar. This changes at 25%CO, where the dense phase is more significantly affected. This behavior at higher impurity concentrations is likely due to the mixture dew point curve occurring at higher pressure than that of pure CO_2.

The MAE calculated between the mixture and pure CO_2, indicates that the effect of CO on density decreases as temperature increases at all analyzed concentrations. Table 9 present these results. This happens because as the temperature increases, the intermolecular interactions of the mixture become less important, causing the fluid to come closer to an ideal gas.

Table 9 – MAE values (kg/m^3) comparing the density of pure CO_2 with the densities of mixtures containing CO at different molar fraction and temperatures.

CO molar fraction	T = 273.15 K	T = 300.15 K	T = 353.15 K
0.03	63.902	47.470	14.520
0.05	101.452	73.583	23.759
0.15	259.457	162.504	65.148
0.25	364.359	224.840	99.680

Source: Prepared by the author.

These same behaviors observed for CO are also evident in the result for the Ar and CH_4 impurities as shown in Figure 17- Figure 21 and Table 10.

Figure 17 – Density behavior for the $CO_2 + Ar$ mixture at 273.15 K.

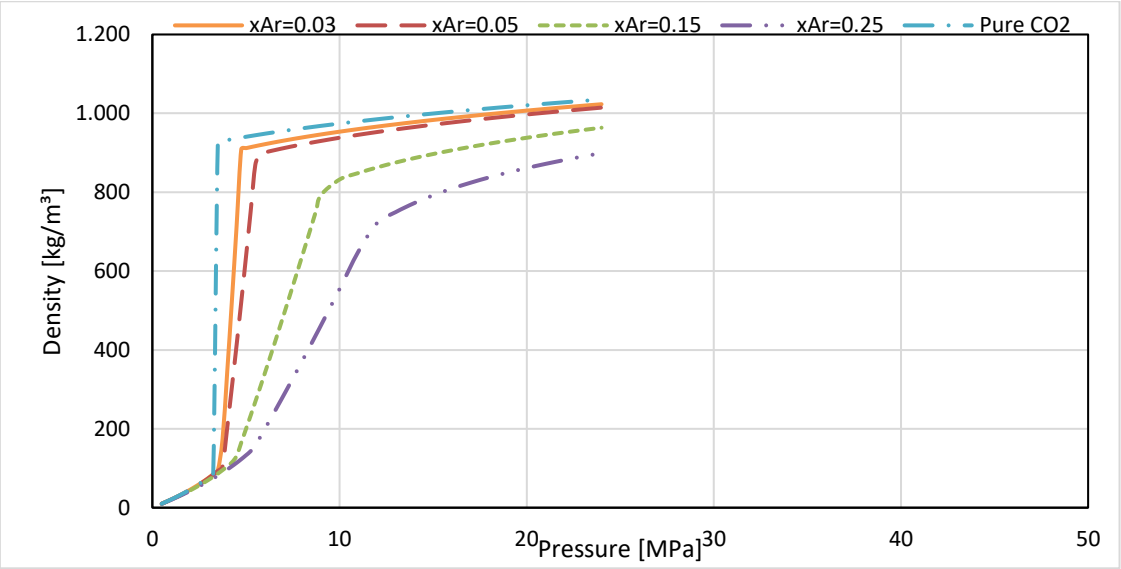

Source: Prepared by the author.

Figure 18 – Density behavior for the $CO_2 + Ar$ mixture at 300.15 K.

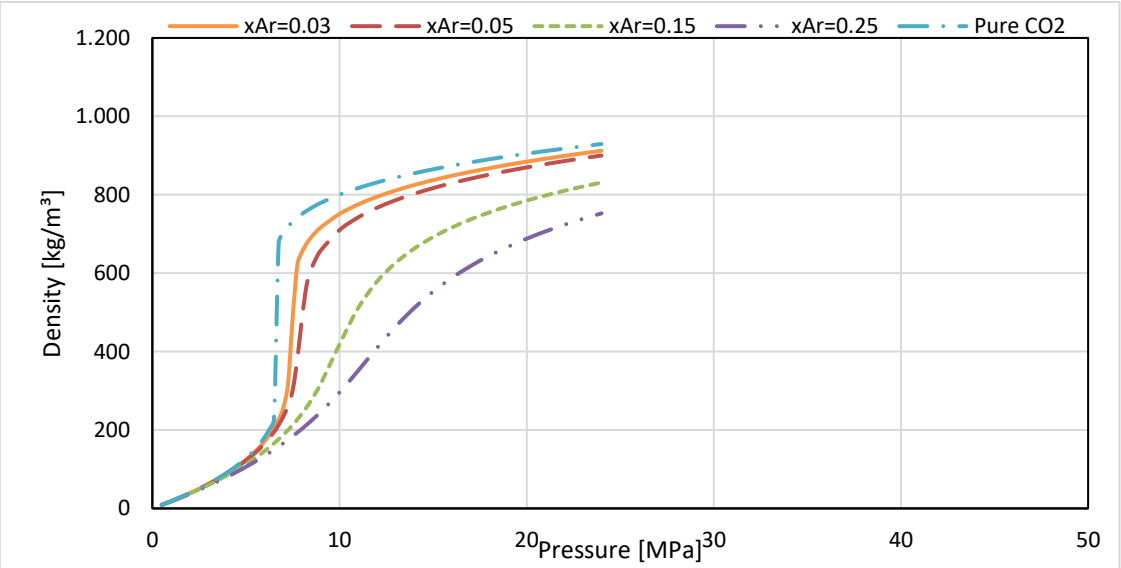

Source: Prepared by the author.

Figure 19 – Density behavior for the $CO_2 + Ar$ mixture at 353.15 K.

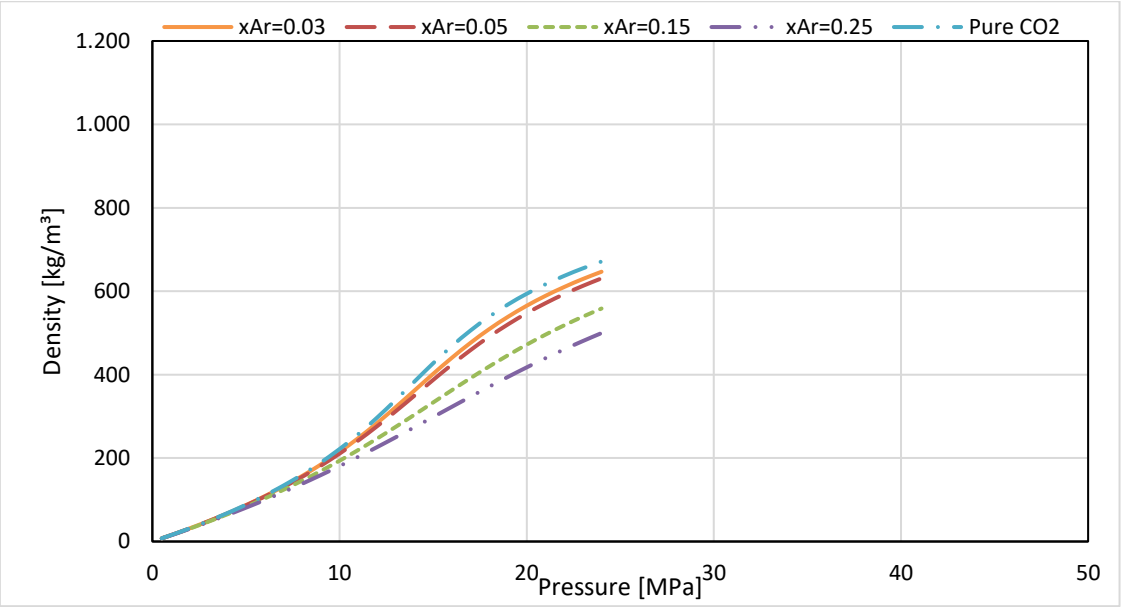

Source: Prepared by the author.

Figure 20 – Density behavior for the $CO_2 + CH_4$ system at 273.15K.

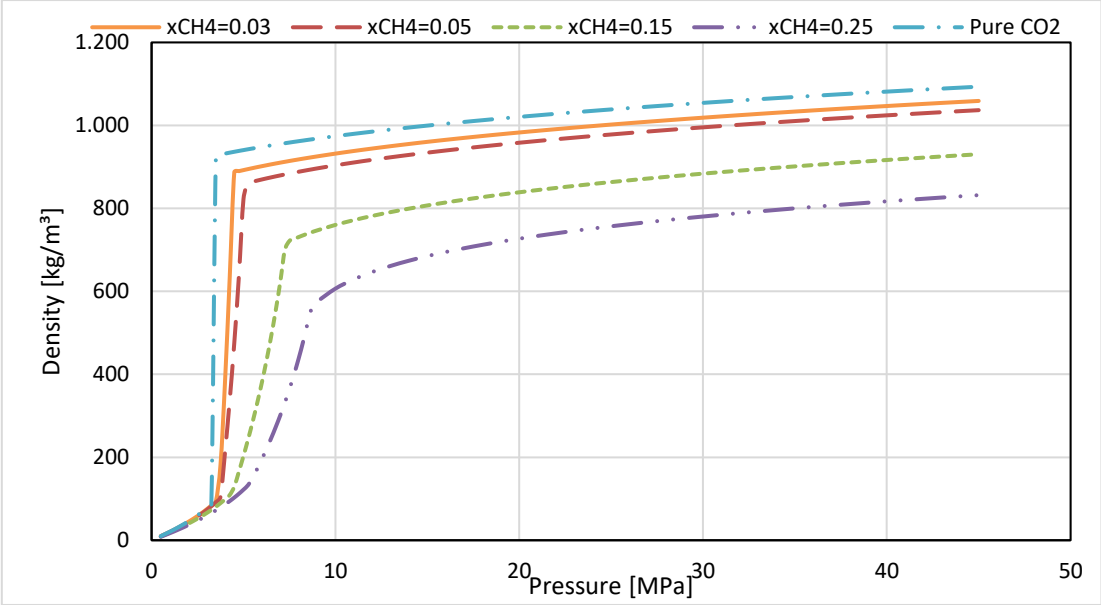

Source: Prepared by the author.

Figure 21 – Density behavior for the $CO_2 + CH_4$ system at 300.15K.

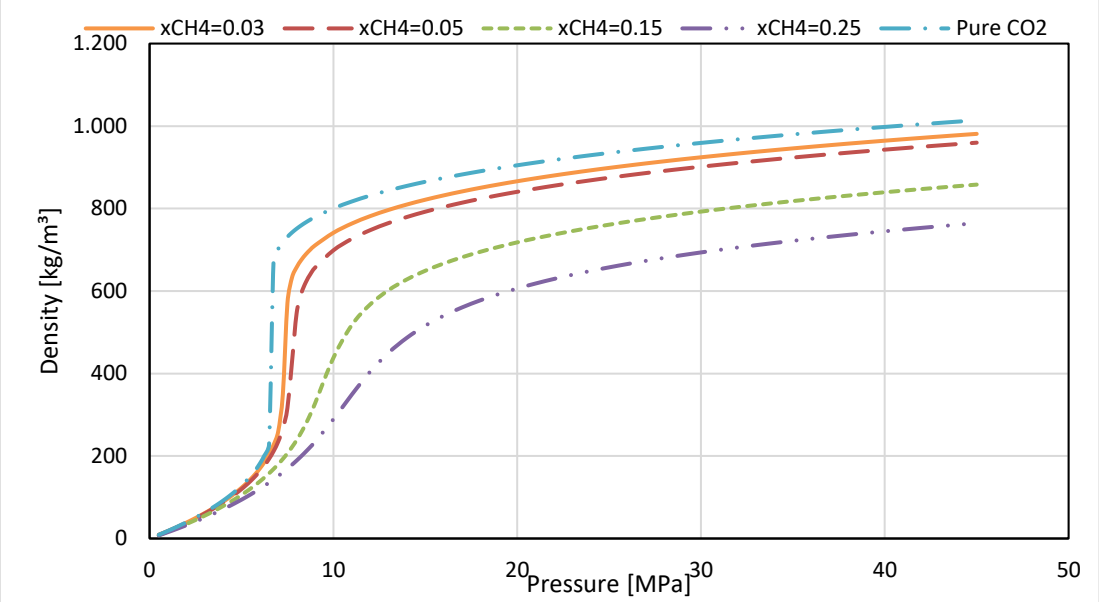

Source: Prepared by the author.

Table 10 – MAE values (kg/m^3) comparing the density of pure CO_2 with the densities of mixtures at different concentrations and temperatures.

Concentration of impurity (%)	T = 273.15 K	T = 300.15 K	T = 353.15 K
	$CO_2 + Ar$		
0.03	71.449	51.741	7.988
0.05	113.169	79.231	12.881
0.15	292.098	161.868	33.059
0.25	398.686	209.093	47.844
	$CO_2 + CH_4$		
0.03	66.183	48.636	-
0.05	104.053	76.129	-
0.15	260.315	173.963	-
0.25	267.613	256.918	-

Source: Prepared by the author.

For both the Ar and CH_4 mixture, the gas phase exhibits the major impact on the density value (Table 11) comparing with CO for 3% and 5%. However, the liquid and dense phase shows a similar behavior as demonstrate by CO.

Table 11 – MAE values (kg/m^3) comparing the density of pure CO_2 with the densities of mixtures at 300.15 K for phase.

CO molar fraction	Gas phase	Liquid phase	Dense phase
	$CO_2 + Ar$		
0.03	37.798	43.307	-
0.05	69.636	68.909	-
0.15	155.929	-	175.330
0.25	180.479	-	280.630
	$CO_2 + CH_4$		
0.03	38.579	44.573	-
0.05	70.440	70.973	-
0.15	141.407	-	201.379
0.25	181.116	-	295.569

Source: Prepared by the author.

Based on MAE values presented in Table 8 and Table 11, CO has the greatest impact on density reduction than Ar. This is shown in Figure 22, which also illustrates the distinct behavior of CH_4 across different phases: in the two-phase region, CH_4 has a smaller impact on density reduction than the other analyzed impurities. However, in the liquid region, it affects the mixture density the most.

Figure 22 – Density behavior of systems with 5% of impurity at 300.15 K.

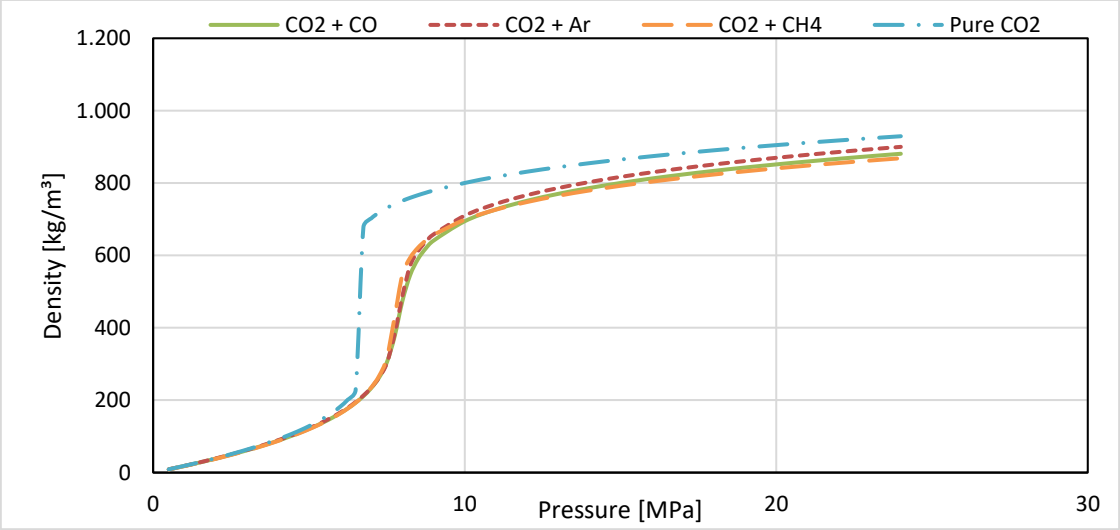

Source: Prepared by the author.

Table 12 present the density reduction rates for each impurity at the studied molar fraction and pressure between 0.5MPa and 45MPa.

Table 12 – Effect of impurities on density reduction compared to pure CO_2 at 300.15 K.

Impurity molar fraction	$CO_2 + CO$	$CO_2 + Ar$	$CO_2 + CH_4$
0.03	-8,96%	-7,98%	-8,84%
0.05	-13,60%	-12,10%	-13,58%
0.15	-27,96%	-24,56%	-29,30%
0.25	-36,81%	-31,83%	-39,21%

Source: Prepared by the author.

This analyze demonstrates that even small presence of impurities in CO_2 fluid, can affect significantly the values of density.

4.2.2 Effect of impurities on phase envelope

Analysis of the systems phase envelope (Figure 23 to Figure 25) reveals that as the fluid transitions from pure CO_2 to a CO_2-rich mixture, a two-phase region develops, and this region becomes more extensive as the impurity concentration increases.

Figure 23 – Phase envelope for $CO_2 + CO$ mixture.

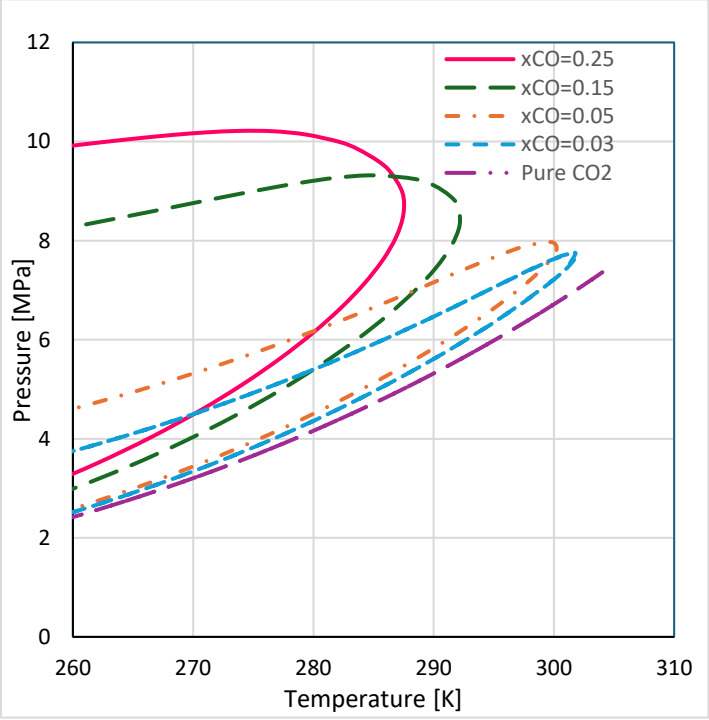

Source: Prepared by the author.

Figure 24 – Phase envelope for $CO_2 + Ar$ mixture.

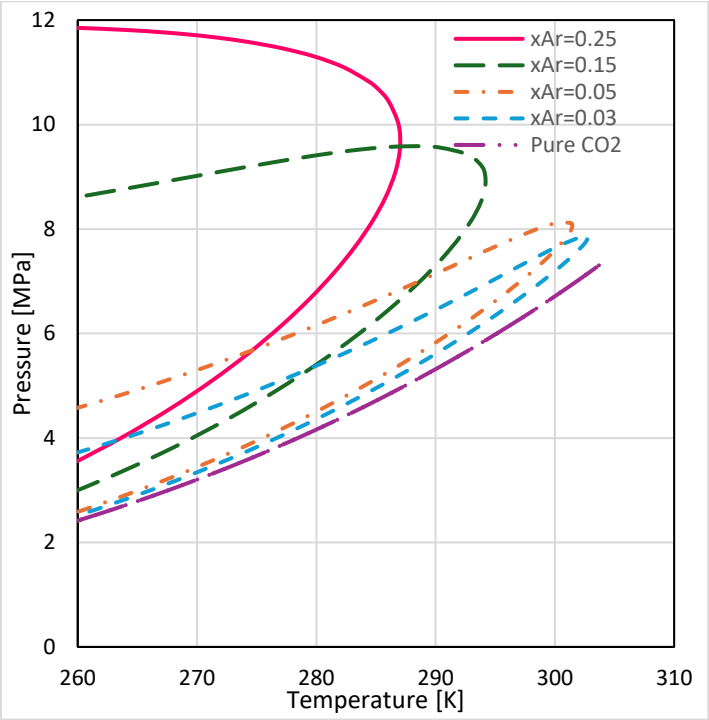

Source: Prepared by the author.

Figure 25 – Phase envelope for $CO_2 + CH_4$ mixture.

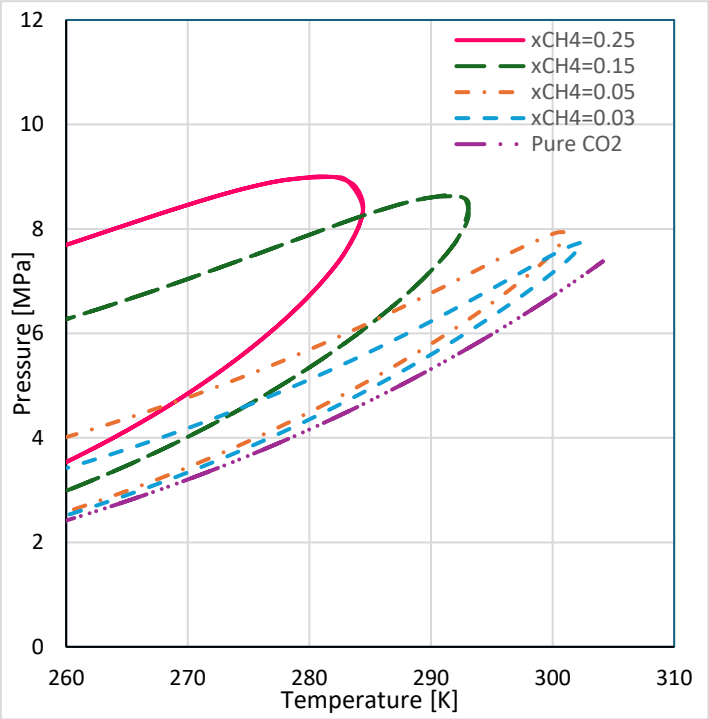

Source: Prepared by the author.

Among the impurities considered, CO exhibits the highest volatility, followed by Ar and then CH_4. More volatile impurities increase the saturation

pressure of the mixture. However, since argon is a noble gas with weaker interactions than CO, it causes an increase in the system's total pressure. This justifies the fact that argon has a more significant impact on the size of two-phase region, while CH_4 has the least impact, generating smaller biphasic regions.

In CCS process, CO_2-rich mixtures is transported through pipelines at pressure exceeding the critical point of pure CO_2, from 8.6MPa to 20MPa, and at ambient temperatures (277.15 K to 311.15 K), which depend on the geographical location (Nazeri et al., 2021). The phase envelope in Figure 23 to Figure 25 reveal a two-phase region under these conditions for higher concentrations of impurities, specially to $CO_2 + Ar$. The critical point also exhibits a change. With increasing molar fraction, it shifts to higher pressures and lower temperatures. The values are shown in Table 13.

Table 13 – Critical points for different concentrations of CO, Ar and CH_4.

Impurity molar fraction	$CO_2 + CO$		$CO_2 + Ar$		$CO_2 + CH_4$	
	P [MPa]	T [K]	P [MPa]	T [K]	P [MPa]	T [K]
0.03	7.74	301.80	7.87	302.77	7.74	302.40
0.05	7.95	300.01	8.11	301.34	7.93	300.96
0.15	9.10	290.10	9.36	293.22	8.63	292.18
0.25	9.85	283.66	10.82	284.42	9.00	281.66
0.00 (pure CO_2)	7.38	304.13	-	-	-	-

Source: Prepared by the author.

CO_2 is typically transported in its supercritical state, as this allows for a greater quantity of fluid to be transferred through smaller diameter pipelines. Additionally, injection CO_2 in its supercritical state into geological formations or oil reservoirs offers advantages, as it makes the process safer and increases CO_2 storage capacity. However, changes in critical points due to the presence of impurities can shift the supercritical region (temperature and pressure conditions). This may require, for example, working with larger diameter pipes or higher pressures, leading to additional costs for the project.

As demonstrate in Table 13 and Figure 26, Ar as an impurity has a critical point at higher pressure and temperature values compared to CH_4 and CO. The critical pressure of CO is higher than the CH_4, but the critical temperature is

inverse. The two-phase region of Ar and CO are very similar and CH_4 exhibiting the smallest region.

Figure 26 – Phase envelope of CO_2-rich mixture with 5% of impurity.

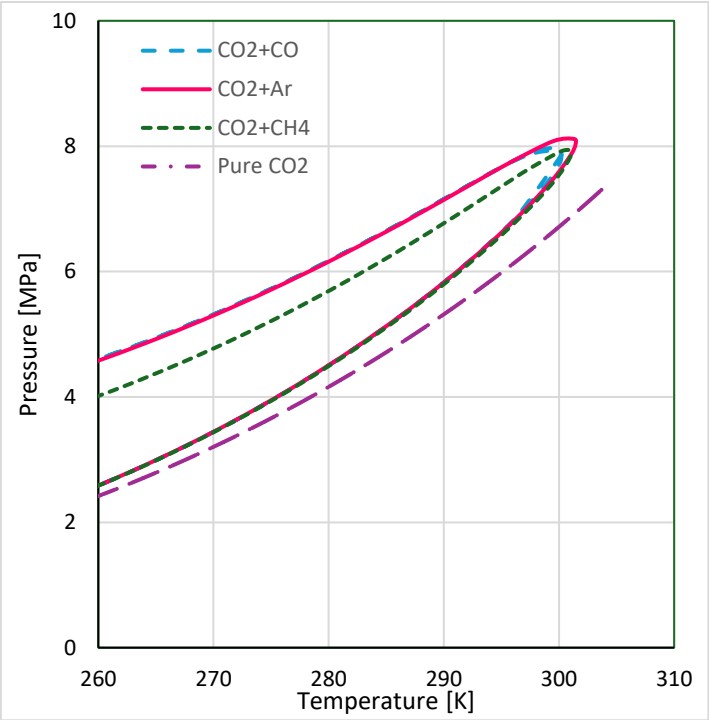

Source: Prepared by the author.

The dew point curves for the three systems containing impurities are very similar, with pressures only slightly above that of pure CO_2. However, the bubble point curve for $CO_2 + CH_4$ has lower pressures than the other mixtures and this directly influences the size of the two-phase region for each analyzes system.

5 CONCLUSION

This study evaluated the impact of adjustments to the GERG-2008 and EOS-CG 2019 equations of state on predicting the density of binary mixture containing CO_2 and impurities (CO, Ar, and CH_4), testing the central hypothesis that adjusting specific parameters would improve prediction accuracy compared to the original models.

For the $CO_2 + CO$ mixture, adjustments to the EOS-CG 2019 formula did not yield any improvements. Compared with the tuned GERG-2008, the original EOS-CG 2019 performed better, with the tuned GERG-2008 outcomes showing a slightly better match against experimental data. However, when a less complex model is necessary, the original EOS-CG 2019 can be a good alternative, skipping the model fitting and obtaining good results with default model parameters values.

GERG-2008 had a more significant tune than the EOS-CG 2019 tune in the $CO_2 + Ar$ mixture. The reduction in statistical errors was greater when compared to the original model. However, EOS-CG 2019 still proved to have better density predictive capacity than GERG-2008.

The model tuning results also showed that the adjustments worked well for the $CO_2 + CH_4$ mixture. Comparison between the models revealed that the adjusted GERG-2008 exhibited lower ARE values for this mixture compared to the EOS-CG 2019 in both its original and adjusted forms, indicating the superiority of the adjusted GERG-2008 for modeling this system.

Overall, regardless of the mixture, GERG-2008 tends to overestimate critical temperatures compared to EOS-CG 2019. This difference increases with increasing impurity concentration. EOS-CG 2019 demonstrates a more consistent performance in critical pressures after adjustment, with minor variations between the different concentrations.

The impurity CO had the most significant impact on reducing density compared to Ar. Besides that, the CH_4 exhibited distinct behavior: in the two-phase region, its impact on density reduction was smaller than that of other analyzed impurities, but in the liquid region, it affected the mixture density the most. The inverse relationship between temperature and density was confirmed,

regardless of CO_2 concentration, and increasing impurity concentration resulted in a decrease in mixture density, as expected. In summary, the presence, type, and concentration of impurities influence the magnitude of the density change.

Phase envelope analysis revealed the impact of impurities on CO_2-Impurity phase behavior, altering the critical point and the bubble and dew point curves. Ar demonstrated the greatest effect on shifting the critical point to higher pressure and temperatures, followed by CH_4 and CO. The impurities also influenced the size of the two-phase region, with CO and Ar resulting in the largest region and CH_4 in the smallest.

5.1 FUTURE RESEARCH SUGGESTIONS

The following suggestions aim to improve the current research by exploring different methods and applications for prediction models of thermodynamic properties of mixtures:

5.1.1 Model optimization and tuning

Future studies should consider the inclusion of an analysis of the magnitude of the errors and the use of further experimental data to optimize and tune the models, as well as the incorporation of equilibrium data. This would ensure better performance of the tuned model under these conditions. In addition, a study on why some parameters of the reducing function had greater adjustments in their values than others are recommended.

5.1.2 Physical-informed Neural Networks approach

Developing a model using PINNs is also a suggestion for future research as it can yield more flexible models. This approach combines physical laws and equations directly into the neural network training, resulting in hybrid models that can be potentially more generalized than classical physical or data-driven models.

5.1.3 Applications in CCS and CCUS

Another important study would be to investigate the impact of impurities on specific applications of CCS and CCUS. This investigation could cover both flowline and flow assurance aspects, assessing how impurities affect the transport and mixture behavior in pipelines and equipment, as well as reservoir engineering, analyzing the impact on CO_2 storage in geological reservoirs and Enhanced Oil Recovery (EOS) techniques.

REFERENCES

About us - GERG. (n.d.). Retrieved February 6, 2025, from https://www.gerg.eu/about-us/#about

Ahmad, A. A., M. Saaid, I., Muhammad, M. A., Husein, N., Zaidin, M. F., & Mohamad Sabil, K. (2023). Physical and chemical effect of impurities in carbon capture, utilisation and storage. *Journal of Petroleum Exploration and Production Technology*, *13*(5), 1235–1246. https://doi.org/10.1007/s13202-023-01616-3

Al-Siyabi, I. (2013). *EFFECT OF IMPURITIES ON CO 2 STREAM PROPERTIES*. Heriot-Watt University.

Arai, Y., Kaminishi, G., & Saito, S. (1971). THE EXPERIMENTAL DETERMINATION OF THE P-V-T-X RELATIONS FOR THE CARBON DIOXIDE-NITROGEN AND THE CARBON DIOXIDE-METHANE SYSTEMS. *Journal of Chemical Engineering of Japan*, *4*, 113–122.

Ben Souissi, M. A., Richter, M., Yang, X., Kleinrahm, R., & Span, R. (2017). Vapor-Phase (p, ρ, T , x) Behavior and Virial Coefficients for the (Argon + Carbon Dioxide) System. *Journal of Chemical & Engineering Data*, *62*(1), 362–369. https://doi.org/10.1021/acs.jced.6b00687

Betts, R., & Keeling, R. (2021, April 7). *Atmospheric carbon dioxide at record high levels despite reduced emissions in 2020*. Met Office. https://www.metoffice.gov.uk/research/news/2021/record-co2-levels-despite-lower-emissions-in-2020

Blanco, S. T., Rivas, C., Bravo, R., Fernández, J., Artal, M., & Velasco, I. (2014). Discussion of the influence of CO and CH4 in CO2 transport, injection, and storage for CCS technology. *Environmental Science and Technology*, *48*(18), 10984–10992. https://doi.org/10.1021/es502306k

Brasil. (2018, August 31). *Acordo de Paris*. Ministério Do Meio Ambiente. https://antigo.mma.gov.br/clima/convencao-das-nacoes-unidas/acordo-de-paris.html

eCycle. (n.d.). *CO2: definição e impactos do dióxido de carbono*. Retrieved July 30, 2023, from https://www.ecycle.com.br/co2/

EPE. (2018, April 4). *Mudanças climáticas e Transição energética*. EPE. https://www.epe.gov.br/pt/abcdenergia/clima-e-energia#:~:text=regi%C3%B5es%20do%20globo%3A-,Por%20que%20a%20temperatura%20m%C3%A9dia%20da%20Terra%20est%C3%A1%20aumentando%3F,de%20efeito%20estufa%20(GEE).

Gao, K., Wu, J., Zhang, P., & Lemmon, E. W. (2016). A Helmholtz Energy Equation of State for Sulfur Dioxide. *Journal of Chemical & Engineering Data*, *61*(8), 2859–2872. https://doi.org/10.1021/acs.jced.6b00195

Gernert, G. J. (2013). *A NEW HELMHOLTZ ENERGY MODEL FOR HUMID GASES AND CCS MIXTURES*. Ruhr-Universität Bochum.

Gernert, J., & Span, R. (2016). EOS-CG: A Helmholtz energy mixture model for humid gases and CCS mixtures. *Journal of Chemical Thermodynamics*, *93*, 274–293. https://doi.org/10.1016/j.jct.2015.05.015

Guedes, T. A. L. (2023). *ANÁLISE DE GARANTIA DE ESCOAMENTO EM LINHAS DE PRODUÇÃO OFFSHORE: MODELAGEM MATEMÁTICA E GERENCIAMENTO DAS CONDIÇÕES DE FORMAÇÃO DE HIDRATOS*. Universidade Federal do Rio de Janeiro.

Herrig, S. (2018). *New Helmholtz-Energy Equations of State for Pure Fluids and CCS-Relevant Mixtures*. Ruhr-Universität Bochum.

IBP. (2023). *Tecnologias de Captura e Armazenamento de Carbono (CCUS) e sua Importância para a Transição Energética no Brasil: o PL 1425*. https://www.ibp.org.br/personalizado/uploads/2023/01/artigo-abc-ccus.pdf

IEA. (2024a, April 25). *Carbon Capture, Utilisation and Storage*. Tracking Carbon Capture, Utilisation and Storage. https://www.iea.org/energy-system/carbon-capture-utilisation-and-storage#tracking

IEA. (2024b, April 25). *Evolution of the CO2 capture project pipeline, 2012-Q1 2024, IEA*. https://www.iea.org/data-and-statistics/charts/evolution-of-the-co2-capture-project-pipeline-2012-q1-2024

IPCC. (2005). *IPCC Special Report on Carbon Dioxide Capture and Storage*.

James, R. (2019). *Quality Guidelines for Energy System Studies: CO2 Impurity Design Parameters*. www.netl.doe.gov

Kestin, J., Kobayashi, Y., & Wood, R. T. (1966). The viscosity of four binary, gaseous mixtures at 20° and 30°C. *Physica*, *32*(6), 1065–1089. https://doi.org/10.1016/0031-8914(66)90143-1

Kortmann, M. (2016). *Development of Empirical Multiparameter Equations of State for Monoethanolamine and Diethanolamine* [Master thesis]. Ruhr-Universität Bochum.

Kunz, O., & Wagner, W. (2012). The GERG-2008 wide-range equation of state for natural gases and other mixtures: An expansion of GERG-2004. *Journal of Chemical and Engineering Data*, *57*(11), 3032–3091. https://doi.org/10.1021/je300655b

Leachman, J. W., Jacobsen, R. T., Penoncello, S. G., & Lemmon, E. W. (2009). Fundamental Equations of State for Parahydrogen, Normal Hydrogen, and Orthohydrogen. *Journal of Physical and Chemical Reference Data*, *38*(3), 721–748. https://doi.org/10.1063/1.3160306

Lemmon, E. W., & Span, R. (2006). Short Fundamental Equations of State for 20 Industrial Fluids. *Journal of Chemical & Engineering Data*, *51*(3), 785–850. https://doi.org/10.1021/je050186n

Liang, X. (2018). Numerical Aspects of Phase Equilibrium Calculations with the Cubic and Association Models. *Industrial & Engineering Chemistry Research*, *57*(42), 14273–14285. https://doi.org/10.1021/acs.iecr.8b03956

Lozano-Martín, D., Akubue, G. U., Moreau, A., Tuma, D., & Chamorro, C. R. (2020). Accurate experimental (p, ρ, T) data of the (CO2 + O2) binary system for the development of models for CCS processes. *The Journal of Chemical Thermodynamics*, *150*, 106210. https://doi.org/10.1016/j.jct.2020.106210

Mantovani, M., Chiesa, P., Valenti, G., Gatti, M., & Consonni, S. (2012). Supercritical pressure–density–temperature measurements on CO2–N2, CO2–O2 and CO2–Ar binary mixtures. *The Journal of Supercritical Fluids*, *61*, 34–43. https://doi.org/10.1016/j.supflu.2011.09.001

McKay, C., Nazeri, M., Haghighi, H., & Erickson, D. (2022). Recommendations for the selection of equation of state during design and operation of impure CO2 transport and storage. *SSRN Electronic Journal*. https://doi.org/10.2139/ssrn.4271532

Mokhatab, S., Poe, W. A., & Mak, J. Y. (2019). Phase Behavior of Natural Gas Systems. In *Handbook of Natural Gas Transmission and Processing* (pp. 37–101). Elsevier. https://doi.org/10.1016/B978-0-12-815817-3.00002-2

Mondal, M. K., Balsora, H. K., & Varshney, P. (2012). Progress and trends in CO2 capture/separation technologies: A review. *Energy*, *46*(1), 431–441. https://doi.org/10.1016/j.energy.2012.08.006

Mortimer, R. G. (2000). Phase Equilibrium. In *Physical Chemistry* (2nd ed., pp. 167–198). Academic Press. https://doi.org/10.1016/B978-012508345-4/50009-5

Nazeri, M., Haghighi, H., Mckay, C., Erickson, D., & Zhai, S. (2021, September 7). Impact of CO2 Specifications on Design and Operation Challenges of CO2 Transport and Storage Systems in CCUS. *SPE Offshore Europe Conference & Exhibition*. https://doi.org/10.2118/205472-MS

Ozaki, M., & Ohsumi, T. (2011). CCS from multiple sources to offshore storage site complex via ship transport. *Energy Procedia*, *4*, 2992–2999. https://doi.org/10.1016/j.egypro.2011.02.209

Pedersen, K. S., Christensen, P. L., & Shaikh, J. A. (2024). *Phase Behavior of Petroleum Reservoir Fluids* (3rd ed.). CRC Press. https://doi.org/10.1201/9780429457418

Porter, R. T. J., Fairweather, M., Pourkashanian, M., & Woolley, R. M. (2015). The range and level of impurities in CO2 streams from different carbon capture sources. *International Journal of Greenhouse Gas Control*, *36*, 161–174. https://doi.org/10.1016/j.ijggc.2015.02.016

Prasad, S. K., Sangwai, J. S., & Byun, H. S. (2023). A review of the supercritical CO2 fluid applications for improved oil and gas production and associated carbon storage. In *Journal of CO2 Utilization* (Vol. 72). Elsevier Ltd. https://doi.org/10.1016/j.jcou.2023.102479

Schmidt, R., & Wagner, W. (1985). A new form of the equation of state for pure substances and its application to oxygen. *Fluid Phase Equilibria*, *19*(3), 175–200. https://doi.org/10.1016/0378-3812(85)87016-3

SEBRAE. (2023, April 6). *Como funciona a comercialização de crédito de carbono?* SEBRAE. https://sebrae.com.br/sites/PortalSebrae/como-funciona-a-comercializacao-de-credito-de-carbono,88dbbc6d15757810VgnVCM1000001b00320aRCRD#:~:text=O%20mercado%20de%20carbono%20caracteriza,mas%20n%C3%A3o%20atingiu%20as%20metas.

Setzmann, U., & Wagner, W. (1991). A New Equation of State and Tables of Thermodynamic Properties for Methane Covering the Range from the Melting Line to 625 K at Pressures up to 1000 MPa. *Journal of Physical and Chemical Reference Data*, *20*(6), 1061–1155. https://doi.org/10.1063/1.555898

Souza, L. F. S., Herrig, S., Span, R., & Trusler, J. P. M. (2019). Experimental density and an improved Helmholtz-energy-explicit mixture model for (CO2 + CO). *Applied Energy*, *251*(113398). https://doi.org/10.1016/j.apenergy.2019.113398

Span, R., Lemmon, E. W., Jacobsen, R. T., Wagner, W., & Yokozeki, A. (2000). A Reference Equation of State for the Thermodynamic Properties of Nitrogen for Temperatures from 63.151 to 1000 K and Pressures to 2200 MPa. *Journal of Physical and Chemical Reference Data*, *29*(6), 1361–1433. https://doi.org/10.1063/1.1349047

Span, R., & Wagner, W. (1996a). A New Equation of State for Carbon Dioxide Covering the Fluid Region from the Triple-Point Temperature to 1100 K at Pressures up to 800 MPa. *Journal of Physical and Chemical Reference Data*, *25*(6), 1509–1596. https://doi.org/10.1063/1.555991

Span, R., & Wagner, W. (1996b). A New Equation of State for Carbon Dioxide Covering the Fluid Region from the Triple-Point Temperature to 1100 K at Pressures up to 800 MPa. *Journal of Physical and Chemical Reference Data*, *25*(6), 1509–1596. https://doi.org/10.1063/1.555991

Spigarelli, B. P., & Kawatra, S. K. (2013). Opportunities and challenges in carbon dioxide capture. *Journal of CO2 Utilization*, *1*, 69–87. https://doi.org/10.1016/j.jcou.2013.03.002

Tegeler, Ch., Span, R., & Wagner, W. (1999). A New Equation of State for Argon Covering the Fluid Region for Temperatures From the Melting Line to 700 K at Pressures up to 1000 MPa. *Journal of Physical and Chemical Reference Data*, *28*(3), 779–850. https://doi.org/10.1063/1.556037

Thol, M., Dubberke, F. H., Baumhögger, E., Span, R., & Vrabec, J. (2018). Speed of Sound Measurements and a Fundamental Equation of State for Hydrogen Chloride. *Journal of Chemical & Engineering Data*, *63*(7), 2533–2547. https://doi.org/10.1021/acs.jced.7b01031

Tomić, L., Karović-Maričić, V., Danilović, D., & Crnogorac, M. (2018). Criteria for CO2 storage in geological formations. *Podzemni Radovi*, *32*, 61–74. https://doi.org/10.5937/PodRad1832061T

Tsankova, G., Stanwix, P. L., May, E. F., & Richter, M. (2017). Densities, Dielectric Permittivities, and Dew Points for (Argon + Carbon Dioxide) Mixtures Determined with a Microwave Re-entrant Cavity Resonator. *Journal of Chemical & Engineering Data*, *62*(9), 2521–2532. https://doi.org/10.1021/acs.jced.6b01043

Wagner, W., & Pruß, A. (2002). The IAPWS Formulation 1995 for the Thermodynamic Properties of Ordinary Water Substance for General and Scientific Use. *Journal of Physical and Chemical Reference Data*, *31*(2), 387–535. https://doi.org/10.1063/1.1461829

Wang, Z., Li, S., Jin, Z., Li, Z., Liu, Q., & Zhang, K. (2023). Oil and gas pathway to net-zero: Review and outlook. In *Energy Strategy Reviews* (Vol. 45). Elsevier Ltd. https://doi.org/10.1016/j.esr.2022.101048

Wegge, R. (2016). *Thermodynamic Properties of the (Argon + Carbon Dioxide) System: Instrument Development and Measurements of Density and Speed of Sound*. Ruhr-Universität Bochum.

Wetenhall, B., Aghajani, H., Chalmers, H., Benson, S. D., Ferrari, M.-C., Li, J., Race, J. M., Singh, P., & Davison, J. (2014). Impact of CO2 impurity on CO2 compression, liquefaction and transportation. *Energy Procedia*, *63*, 2764–2778. https://doi.org/10.1016/j.egypro.2014.11.299

Yang, X., Richter, M., Wang, Z., & Li, Z. (2015). Density measurements on binary mixtures (nitrogen + carbon dioxide and argon + carbon dioxide) at temperatures from (298.15 to 423.15) K with pressures from (11 to 31) MPa using a single-sinker densimeter. *The Journal of Chemical Thermodynamics*, *91*, 17–29. https://doi.org/10.1016/j.jct.2015.07.014

Yu, J., Du, X., Hao, T., Zhu, W., Yuan, X., Wu, J., & Xu, Q. (2025). Review of Physical Properties of High Carbon Dioxide Content. *Applied and Computational Engineering*, *127*(1), 187–192. https://doi.org/10.54254/2755-2721/2025.20174

Zhang, T., Sun, S., & Bai, H. (2022). Thermodynamically-consistent flash calculation in energy industry: From iterative schemes to a unified thermodynamics-informed neural network. *International Journal of Energy Research*, *46*(11), 15332–15346. https://doi.org/10.1002/er.8234

APPENDIX A – CARBON DIOXIDE + CARBON MONOXIDE SYSTEM ($CO_2 + CO$)

A.1 GERG-2008

In the original GERG-2008 formulation (Equation 10), the binary interaction parameters of the reducing function for volume (β_v and γ_v) and temperature (β_T and γ_T) for $C0_2 + CO$ mixture are unity. Furthermore, the F_{ij} parameter is set to zero, and the default Lorentz-Berthelot combining rule is applied. Although the original model already considers this mixture, the parameters of the reducing function do not incorporate specific tuning for these terms, and therefore, it may represent an opportunity for model parameter improvement (Kunz & Wagner, 2012). Thus, it will be possible to evaluate the performance of a model specifically adjusted for the CO impurity.

During the simulations, a set of combinations (Figure 11) of adjustable parameters were tested for two training dataset (composed by 1030 data each). This study aimed to identify the combination that best fitted to the experimental data, using the error values (ARE, MAE and RMSE) for analysis. These results are presented in Table A1.

Table A1– Performance of fitting parameters combinations of GERG-2008 for $CO_2 + CO$ training set (1030 data). The combinations of adjustment are identified in the Table 5. The best results are highlighted in bold.

Combination of adjustment [-]	Dataset 1			Dataset 2		
	ARE [%]	MAE $[kg/m^3]$	RMSE $[kg/m^3]$	ARE [%]	MAE $[kg/m^3]$	RMSE $[kg/m^3]$
1	3.363	18.488	43.618	3.414	19.592	46.403
2	3.605	19.227	43.656	3.651	20.356	46.331
3	3.562	19.175	**43.297**	3.628	20.358	**46.052**
4	3.243	18.144	43.952	**3.336**	**19.358**	46.594
5	3.365	18.493	43.615	3.414	19.593	46.402
6	3.604	19.225	43.651	3.653	20.358	46.349
7	**3.242**	**18.140**	43.951	3.337	19.363	46.593
Average	**3.426**	**18.699**	**43.677**	3.490	19.854	46.389

Source: Prepared by the author.

Dataset 1 presented the lowest average ARE in relation to the training data. This result indicates that the model fitted on dataset 1 provided a better representation of the experimental densities used in the adjustment process. This

similarity in error values indicates that the dataset of experimental densities used is not biased.

An analysis of the different adjustment combinations revealed that including the F_{ij} parameter did not result in significant improvements in the model adjustments. This is noticed since the combinations 1 and 5, 2 and 6, and 4 and 7 have very similar results and their only difference is the presence of F_{ij} in the adjustment.

For the $CO_2 + CO$ mixture, the minimal influence of F_{ij} on the representation of thermodynamic properties for the dataset investigated (described in section 3.3), suggests that the model may already be optimized with original value of F_{ij} or additional experimental data with different thermodynamic properties, beyond density, may be needed for further refinement.

Furthermore, for this same dataset considered, it was found that the adjustment in the parameters related to temperature ($\beta_{T,ij}$ and $\gamma_{T,ij}$) presents lower error values than those related to volume. This can be observed by comparing combinations 1 with 2, and 5 with 6.

Both dataset 1 and dataset 2 exhibited similar statistical results in Table A1, which is advantageous as it indicates a consistent pattern across different datasets. This consistency in the results indicates that they are reliable and suggests that the trends are not dependent on a single dataset.

For both dataset, combinations 4 and 7 demonstrated the best performance, with very similar ARE and MAE values. However, combination 4 was selected for subsequent analyses because it achieved similar error values while requiring the adjustment of fewer parameters than combination 7. The resulting parameter values for combinations 4 are presented in Table A2 .

The parameters $\beta_{T,ij}$ and $\beta_{v,ij}$ showed the largest adjustments, with their values being reduced by a little more than double (106.3% and 112.0%, respectively). The values of $\gamma_{T,ij}$ and $\gamma_{v,ij}$ were also changed, but with a smaller rate of variation compared to the $\beta_{T,ij}$ and $\beta_{v,ij}$. The change in $\gamma_{v,ij}$ was less than 1% while $\gamma_{T,ij}$ had a readjustment of approximately 10%.

Table A2 – The values of the adjustable parameters of the GERG-2008 for $CO_2 + CO$ after the tuning process.

Parameters	Before tune	Dataset 1	Dataset 2
		After tune	After tune
$\beta_{T,ij}$	1	-0.06530111	-0.12201317
$\gamma_{T,ij}$	1	1.10873413	1.09504533
$\beta_{v,ij}$	1	-0.09590386	-0.20361099
$\gamma_{v,ij}$	1	1.00287712	1.00689328
F_{ij}	0	0	0

Source: Prepared by the author.

To evaluate the GERG-2008 model's fitting, statistical errors were calculated before and after tuning, comparing the model density estimates against the experimental data for each validation dataset (composed by 340 data each). This step is crucial for verifying the model's predictive capability on data excluded in the adjustment process and allows for a robust assessment of the fitted model generalization. Table A3 presents the average values of ARE, MAE, and RMSE for density data.

Table A3 – Error values calculated for the validation set (340 data) of the $CO_2 + CO$ mixture for the GERG-2008. The best results are highlighted in bold. Calculated errors based on density values.

	Validation set 1		Validation set 2	
	Before tune	After tune	Before tune	After tune
ARE [%]	3.362	**3.082**	3.161	**2.919**
MAE [kg/m^3]	12.593	**11.343**	9.597	**8.554**
RMSE [kg/m^3]	31.878	**31.761**	24.860	**24.738**

Source: Prepared by the author.

Based on the fitted parameters, the GERG-2008 model demonstrated a very slight improvement in the error indicators. The ARE values decreased by 0.280% and 0.242% for validation set 1 and 2, respectively. Although validation set 1 showed a slightly higher ARE reduction rate, validation set 2 still exhibits lower final ARE values, indicating that the model fit for this validation set better represented the experimental data considered in this study.

The small variation in RMSE values indicates that the model showed improvement in most of the errors, as evidenced by the ARE and MAE. However,

the model still has problems in adjusting outliers' values. This issue can be observed in Figure A1, where the points farthest from the reference line of the experimental data represent the outliers.

Figure A1 – Simulated density versus experimental density for the system $CO_2 + CO$ using the fitted model of the GERG-2008.

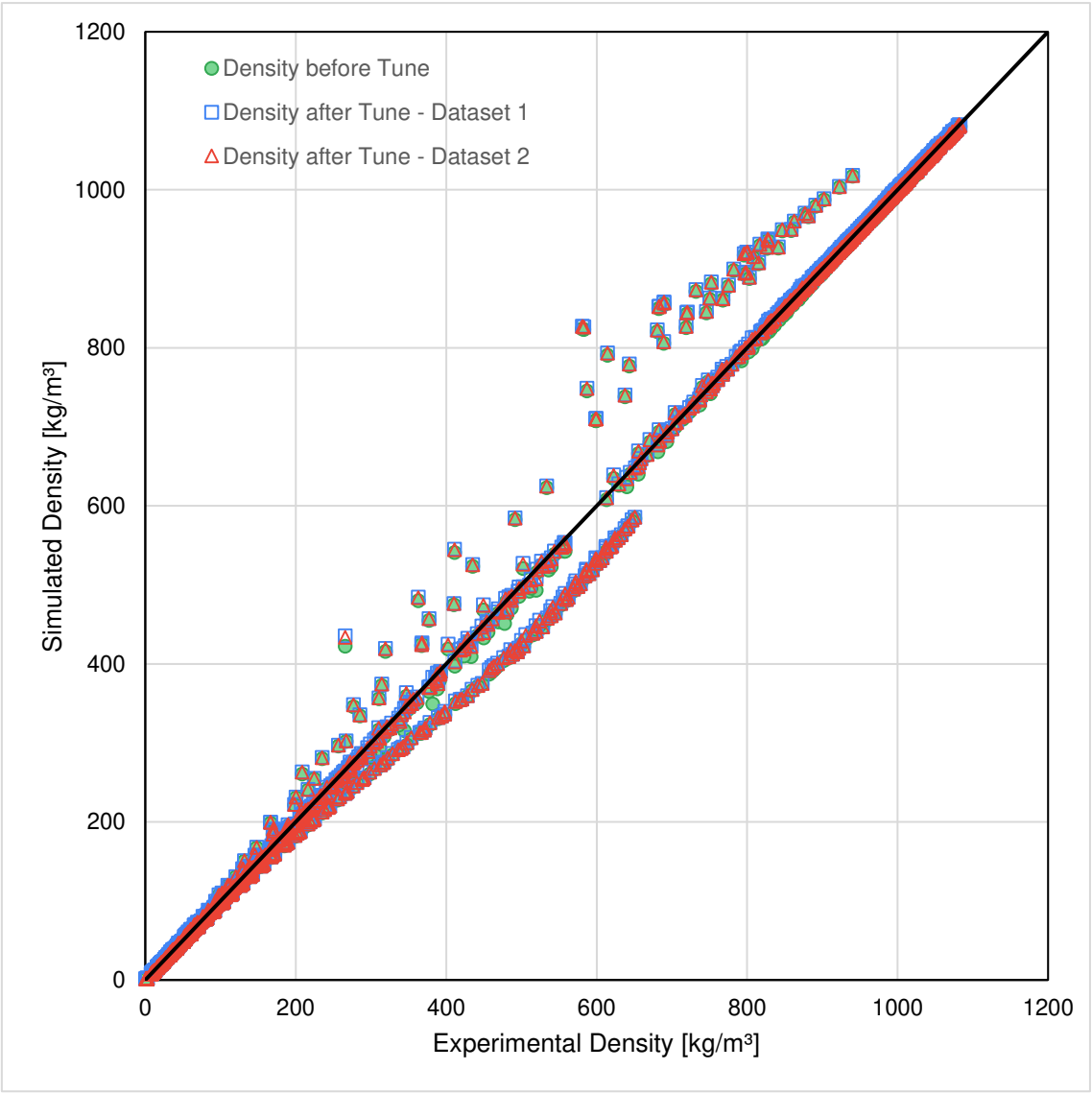

Source: Prepared by the author.

Figure A1 shows how closely the simulated densities match the experimental densities using the complete dataset (training and validation set) of $CO_2 + CO$, and also highlighting the similar performance of the adjusted and original model. It is worth emphasizing that the pressure and temperature ranges of the data used in this analysis are within range of pressure and temperature conditions considered in the original GERG-2008 model.

After analyzing the data, it was observed that the densities related to higher pressure values presented the highest MAE values, represented by some outliers in Figure A1. Other cases of outliers may occur when the original model predicts the fluid in one phase and the adjusted model in another or even in two-phase region.

Because the presence of impurities in the CO_2 fluid affects the properties of the mixture, and this influence can be intensified according to the concentration of these impurities. Table A4 specifies the results by mole fraction range of the CO impurity. Within these ranges, only impurity concentration values relevant to CCS operational processes were considered.

Table A4 – Error values for the $CO_2 + CO$ density for each impurity molar fraction before and after the GERG-2008 tuning. The best results are highlighted in bold.

CO molar [%]	Num. of data	ARE [%]		MAE [kg/m^3]		RMSE [kg/m^3]	
		Before	After	Before	After	Before	After
Dataset 1							
0% up to 1%	736	2.381	**2.322**	7.107	**6.631**	377.370	**361.825**
1% up to 3%	527	5.334	**5.039**	21.718	**20.120**	**1980.4**	1993.9
3% up to 5%	107	2.636	**0.542**	6.135	**1.051**	79.407	**2.845**
Dataset 2							
0% up to 1%	736	2.381	**2.325**	7.107	**6.668**	377.370	**363.812**
1% up to 3%	527	5.334	**5.058**	21.718	**20.195**	**1980.4**	1989.5
3% up to 5%	107	2.636	**0.813**	6.135	**1.517**	79.407	**4.858**

Source: Prepared by the author.

For the range of 1% to 3%, the tuned models presented larger errors, resulting from a specific selection of experimental data (1.01% CO from SOUZA et al. (2019) data) that showed systematically lower efficacy compared to the other studied dataset. The errors were smaller for the CO molar fraction between 3% and 5%, and it is worth highlighting at this point the significant reduction in RMSE values, indicating that, for this concentration range, the tuned models were able to better describe the points with outliers. This is an important finding, since when the studying fluid indicates these CO concentrations in CO_2 fluids, these adjusted models can be a good option for predicting densities.

To understand the impact of the fitted GERG-2008 model parameters on the mixture critical point, the critical temperatures and pressures estimates were compared before and after tuning and transcribed to Table A5. The model parameters obtained in the adjustment using dataset 1 showed smaller deviations from the original model compared to the dataset 2 adjustment.

Table A5 – Simulated critical points before and after the adjustments of the GERG-2008 model for the $CO_2 + CO$.

CO molar [%]	Original Before tune		Dataset 1 After tune		Dataset 2 After tune	
	T_C [K]	P_C [MPa]	T_C [K]	P_C [MPa]	T_C [K]	P_C [MPa]
3%	304.473	8.367	303.561	8.019	303.650	8.063
5%	303.937	8.915	302.657	8.369	302.788	8.437
15%	298.253	11.516	295.939	9.914	296.112	10.102
25%	288.032	14.642	286.601	11.431	286.587	11.755

Source: Prepared by the author.

Regarding the discrepancy in the determination of critical pressure values after tuning compared to before tuning, it was observed that for 3%CO the average change in the two dataset was 3.90% (for less) and for 25%CO this average was 21% (for less). This shows that the difference between the original and tuned model increases the higher the impurity concentration. Regarding the critical temperature, the deviations were less than 1%, also with the tendency to increase with the increase in CO presence, except at 15%, which has a larger deviation than 25%. In general, a justification for the deviations increasing along with the molar fraction of the impurity is that the impurity increases the complexity of the phase equilibrium due to the expansion of the two-phase region, causing the saturation curves to shift and, consequently, the critical point.

In general, the model tuned from dataset 2 was able to better predict the densities compared to the experimental data used in this study. However, based on the error values, the adjustments were still small when compared to the original model, although they showed good results for CO molar fractions between 3% and 5%. Thus, in case of needing to use GERG-2008 with a slightly improved accuracy, the adjustment can be applied.

A.2 EOS-CG 2019

Unlike GERG-2008, the original EOS-CG 2019 was developed considering the $CO_2 + CO$ mixture, incorporating adjusted values for the binary parameters of the reducing functions and employing a specific departure function (unitary) (Herrig, 2018). An adjustment to this model would be to study the viability of further refining the already tuned parameters or to understand the influence of adjusting the F_{ij} parameter on the predictive capacity of the densities.

Table A6 details the simulation results obtained for each combination of adjusted parameters applied to both training datasets. A comparison of the average error values reveals that dataset 1 performed slightly better than dataset 2. The proximity of the error values between the datasets again indicates that there is not biasing on the results.

Table A6 – Performance of fitting parameters combinations of EOS-CG 2019 for $CO_2 + CO$ training set (1030 data). The combinations of adjustment are identified in the Table 5. The best results are highlighted in bold. Calculated errors based on density values.

Combination of adjustment	Dataset 1			Dataset 2		
	ARE [%]	MAE $[kg/m^3]$	RMSE $[kg/m^3]$	ARE	MAE $[kg/m^3]$	RMSE $[kg/m^3]$
1	4.356	18.167	**43.576**	4.324	19.239	**46.328**
2	3.234	**18.095**	43.858	**3.284**	**19.120**	46.524
3	**3.227**	18.153	43.960	3.287	19.247	46.648
4	3.247	18.324	44.021	3.285	19.189	46.593
5	3.429	18.722	43.642	3.480	19.842	46.444
6	3.239	18.284	44.037	3.311	19.432	46.700
7	3.270	18.286	43.972	3.339	19.400	46.603
Average	**3.429**	**18.290**	**43.867**	3.473	19.353	46.549

Source: Prepared by the author.

From the results in Table A6, it was identified that the adjustment of the F_{ij} parameter combined with other parameters (combinations 5, 6 and 7) did not present errors slightly higher than those in which the F_{ij} is not adjusted (combinations 1, 2 and 4). In addition, it was found that the $\beta_{v,ij}$ and $\gamma_{v,ij}$ parameters present better results when adjusted than the $\beta_{T,ij}$ and $\gamma_{T,ij}$ parameters (comparison of combinations 1 with 2, and 5 with 6).

For dataset 1, the combination of adjustments that best described the experimental densities was 3, where ARE and MAE values are among the lowest. Combination 3 adjusts only the F_{ij} parameter. Given that the original model already features adjusted parameters for the reducing function, refining F_{ij} is a logical approach. In dataset 2, combination 2 was selected because it presents the lowest values of ARE and MAE for this dataset. Parameter values before and after tune for the selected combinations are shown in Table A7.

Table A7 – The values of the adjustable parameters of the EOS-CG 2019 for $CO_2 + CO$ after the tuning process.

Parameters	Before tune	Dataset 1	Dataset 2
		After tune	After tune
$\beta_{T,ij}$	0.9897820	0.9897820	0.9897820
$\gamma_{T,ij}$	1.1621298	1.1621298	1.1621298
$\beta_{v,ij}$	1.0338017	1.0338017	-0.0585527
$\gamma_{v,ij}$	1.0001623	1.0001623	0.96895838
F_{ij}	1	0.7929688	1

Source: Prepared by the author.

For the dataset 1, F_{ij} value was reduced by 20.70%, while in dataset 2 $\beta_{v,ij}$ parameter was reduced by 105.67% and $\gamma_{v,ij}$ by only 3.12%.

Analysis of the error values (Table A8) with validation set indicates that the adjustment did not enhance the predictive capacity of the model, resulting in slightly increased errors compared to the original model. This outcome suggests that the model already provides a good representation of this mixture and an adjustment may not be necessary.

Table A8 – Error values calculated for the validation set (340 data) of the $CO_2 + CO$ mixture using the EOS-CG 2019. The best results are highlighted in bold. Calculated errors based on density values.

	Validation set 1		Validation set 2	
	Before tune	After tune	Before tune	After tune
ARE [%]	**3.068**	3.078	**2.882**	2.886
MAE [kg/m^3]	**11.330**	11.336	**8.492**	8.499
RMSE [kg/m^3]	**31.698**	31.735	24.734	**24.733**

Source: Prepared by the author.

As previously stated, the tuned model based on both the validation sets had an increase in error values, for validation set 1, ARE was 0.01% more and for validations set 2 it was 0.004% being the tune that deviated the least from the original model and also the one that presented the lowest statistical error values.

Turning across the complete $CO_2 + CO$ dataset (training and validation sets) demonstrated that the original EOS-CG 2019 predicted densities as the original EOS-CG 2019 for CO and that the fit results are not significantly difference between the two dataset. These results are presented in Figure A2.

Figure A2 – Simulated density versus experimental density for the system $CO_2 + CO$ using the fitted model of the EOS-CG 2019.

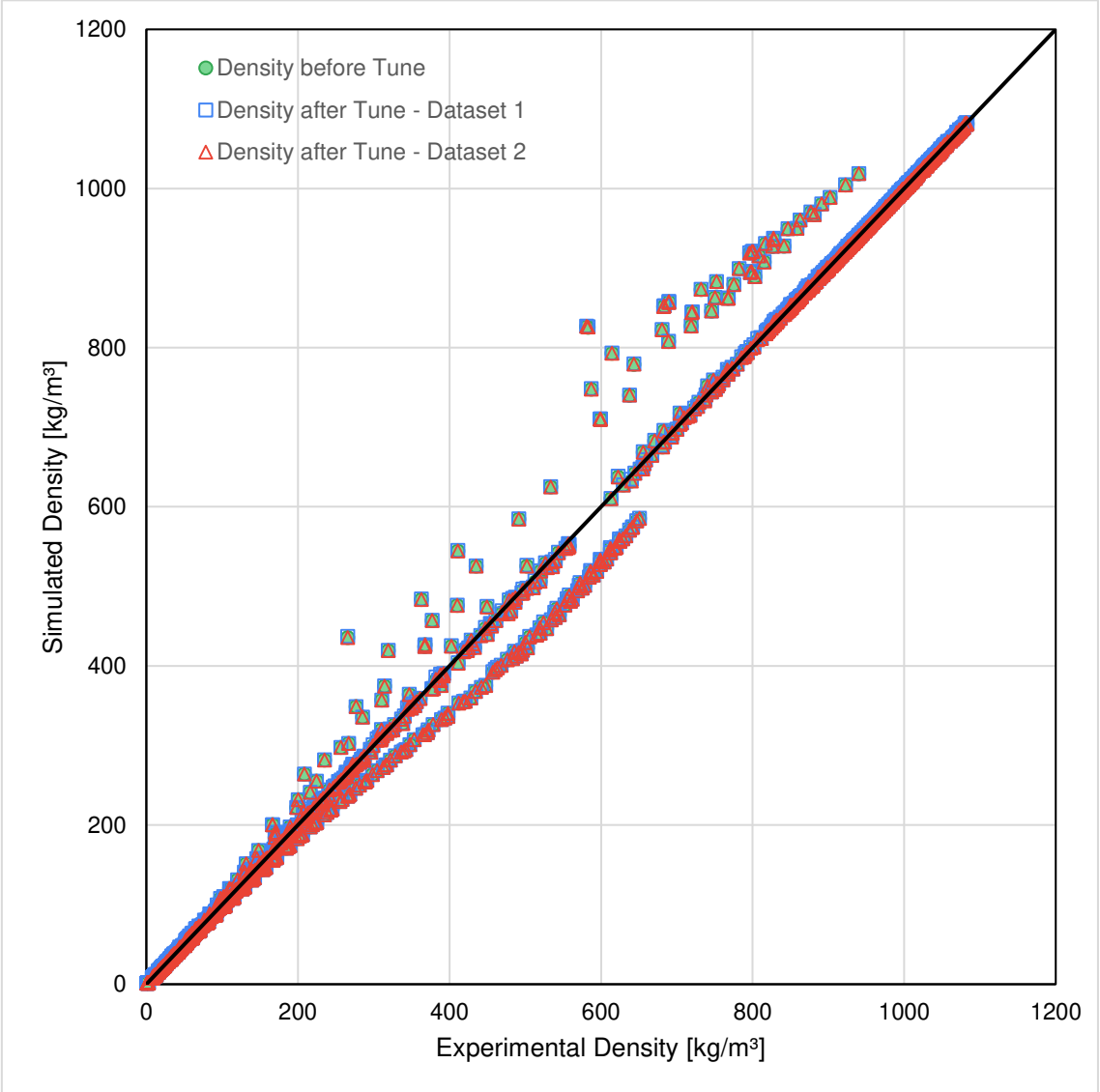

Source: Prepared by the author.

Similarly in the GERG-2008 analysis, the EOS-CG 2019 also have some points differed from the analyzed set (dispersion far from the reference line), where the hypotheses for this are also the same, that is, prediction of density in different phases.

By analyzing the errors for different CO molar fraction ranges in Table A9, it was possible to observe that, for the tune generated by both dataset 1 and 2, for concentrations in the range of 3% to 5%, the errors were higher for the tuned model. For the other ranges, the values are smaller, but the difference is almost negligible.

Table A9 – Error values for the $CO_2 + CO$ data for each impurity molar fraction before and after the EOS-CG 2019 tuning. The best results are highlighted in bold. Calculated errors based on density values.

CO molar [%]	Num. of data	ARE [%]		MAE [kg/m^3]		RMSE [kg/m^3]	
		Before	After	Before	After	Before	After
Dataset 1							
0% up to 1%	736	2.295	**2.290**	6.687	**6.628**	363.169	**361.301**
1% up to 3%	527	5.028	**5.019**	20.113	**20.054**	**1984.6**	1992.2
3% up to 5%	107	**0.227**	0.378	**0.444**	1.017	**0.673**	2.764
Dataset 2							
0% up to 1%	736	2.295	2.295	6.687	**6.680**	363.169	**363.145**
1% up to 3%	527	**5.028**	5.029	**20.113**	20.129	**1984.6**	1989.3
3% up to 5%	107	**0.227**	0.262	**0.444**	0.640	**0.673**	1.298

Source: Prepared by the author.

The range of 1% up to 3% presents the same effect felt for GERG-2008 for this mixture, with more altered values. However, it is worth highlighting that for the range of 3% up to 5% the model has an excellent performance, with error values lower than 1% in the case of the original model, being able to reduce the effect of outliers in the experimental data used (referenced by RMSE).

For the EOS-CG 2019, the adjustment with dataset 2 showed critical temperature and pressure values very close to those of the original model, as seen in Table A10. In dataset 1, the critical temperature and pressure values are slightly higher than those of original model.

Table A10 – Simulated critical points before and after the adjustments of the EOS-CG 2019 model for the $CO_2 + CO$.

CO molar [%]	Original Before tune		Dataset 1 After tune		Dataset 2 After tune	
	T_C [K]	P_C [MPa]	T_C [K]	P_C [MPa]	T_C [K]	P_C [MPa]
3%	301.819	7.742	302.153	7.772	301.700	7.753
5%	299.995	7.949	300.500	7.984	299.990	7.947
15%	290.128	9.103	291.396	9.165	290.281	9.120
25%	278.754	10.389	280.864	10.410	279.402	10.475

Source: Prepared by the author.

For the critical temperature, it was observed that the deviation between the prediction of the original model and the tuned models increases the greater the presence of CO (varying on average from 0.04% for 3% CO and 0.49% for 25% CO). The critical pressure presented deviations of less than 1% (for GERG-2008 the smallest average deviation was 3.90%).

The model tuned from validation set 2 was able to predict the densities better compared to the validation set 1. However, based on the error values, the tunes do not present advantages in the model's behavior, confirming that it already describes the $CO_2 + CO$ system very well.

APPENDIX B - CARBON DIOXIDE + ARGON SYSTEM ($CO_2 + Ar$)

B.1 GERG-2008

In contrast to CO, the original GERG-2008 already includes adjusted binary interaction parameters for the reducing function for volume (β_v e γ_v) and temperature (β_T e γ_T) for the $CO_2 + Ar$ mixture. However, the F_{ij} parameter is also defined as zero, and this presents an opportunity for improvement to be explored in this study (Kunz & Wagner, 2012).

The simulations showed better results for argon as an impurity compared to CO, based on error values, as seen in Table B1, which shows the result for both dataset and for each combinations of adjustment.

Table B1 – Performance of fitting parameters combinations of GERG-2008 for $CO_2 + Ar$ training set (369 data). The combinations of adjustment are identified in the Table 5. The best results are highlighted in bold. Calculated errors based on density values.

Combination of adjustment [-]	Dataset 1			Dataset 2		
	ARE [%]	MAE $[kg/m^3]$	RMSE $[kg/m^3]$	ARE [%]	MAE $[kg/m^3]$	RMSE $[kg/m^3]$
1	1.196	5.157	10.676	1.198	5.050	10.752
2	1.508	6.893	14.331	1.504	6.654	14.412
3	1.330	6.149	12.570	1.316	5.946	12.567
4	1.066	4.339	9.206	0.861	3.177	6.892
5	1.196	5.160	10.683	1.197	5.049	10.749
6	1.508	6.893	14.330	1.503	6.651	14.396
7	**0.993**	**3.878**	**8.255**	**0.866**	**3.192**	**6.922**
Average	1.257	5.496	11.436	**1.206**	**5.103**	**10.956**

Source: Prepared by the author.

For this system, according to the results of the statistical errors, the tune carried out using the training data from dataset 2 indicates that it had a better capacity to predict densities than those from dataset 1.

The combinations that adjusted the parameters $\beta_{T,ij}$ and $\gamma_{T,ij}$ (combinations 1 and 5) presented smaller errors than the combinations that adjusted the parameters $\beta_{v,ij}$ and $\gamma_{v,ij}$ (combinations 2 and 6). This indicates that tune had a greater influence on the parameters related to temperature. This same behavior was observed in the GERG-2008 analysis for the $CO_2 + CO$ mixture (in Appendix A).

The impact of the F_{ij} adjustment proved to be more significant when adjusted together with the $\beta_{T,ij}$, $\gamma_{T,ij}$, $\beta_{v,ij}$ and $\gamma_{v,ij}$ parameters simultaneously (comparison between combination 4 and 7). In other situations, F_{ij} adjustment does not demonstrate a real improvement in the model's predictive capacity.

For both dataset, combinations 4 and 7 demonstrated the best adjustment performance (Table B1). Combination 4 adjusts parameters of the reducing function only, which are already adjusted in the original model. However, combination 7 adjust both the reducing function parameters and, additionally, the F_{ij}. Combination 7 was selected because it adjust terms that are zero in the original model and the new parameters values for this combination are shown on Table B2.

Table B2 – The values of the adjustable parameters of the GERG-2008 for $CO_2 + Ar$ after the tuning process.

Parameters	Before tune	Dataset 1	Dataset 2
		After tune	After tune
$\beta_{T,ij}$	0.99651286	0.99651286	-0.43660575
$\gamma_{T,ij}$	1.05097164	1.036491275	1.03208709
$\beta_{v,ij}$	1.00839243	1.00839243	-0.08452512
$\gamma_{v,ij}$	1.02920546	1.047390223	1.07445371
F_{ij}	0	0.00003652	0.00834872

Source: Prepared by the author.

Among the adjusted values, the β parameters related to both volume and temperature showed the greatest variations. While the departure function was also adjusted, the change in its value was relatively minor. However, this adjustment led to a 0.53% improvement in the ARE compared to the original model for validation set 2, as presented in Table B3.

The GERG-2008 tuning for $CO_2 + Ar$ mixture allowed for a fine adjustment of the model's predictive capability for densities. The ARE was reduced by an average of 0.42%, with the tuning using validation set 2 showing the best results. MAE values were also reduced by a considerable amount, reaching almost 50% for the tune with validation set 2 when compared to experimental densities.

Table B3 – Error values calculated for the validation set (121 data) of the $CO_2 + Ar$ mixture for the GERG-2008. The best results are highlighted in bold. Calculated errors based on density values.

	Dataset 1		Dataset 2	
	Before tune	After tune	Before tune	After tune
ARE [%]	1.260	**0.951**	1.292	**0.764**
MAE [kg/m^3]	6.142	**3.815**	6.706	**3.398**
RMSE [kg/m^3]	13.215	**8.633**	13.168	**7.005**

Source: Prepared by the author.

Based on Figure B1 and Table B3 through RMSE it can be stated that the data in this dataset have a lower quantity of outliers than for $CO_2 + CO$ mixture, since RMSE with presence of argon is lower. Additionally, Figure B1 also evidences that GERG-2008, after being adjusted in both analyzed datasets, presents a better results than before when compared to experimental densities.

Figure B1 – Simulated density versus experimental density for the system $CO_2 + Ar$ using the fitted model of the GERG-2008.

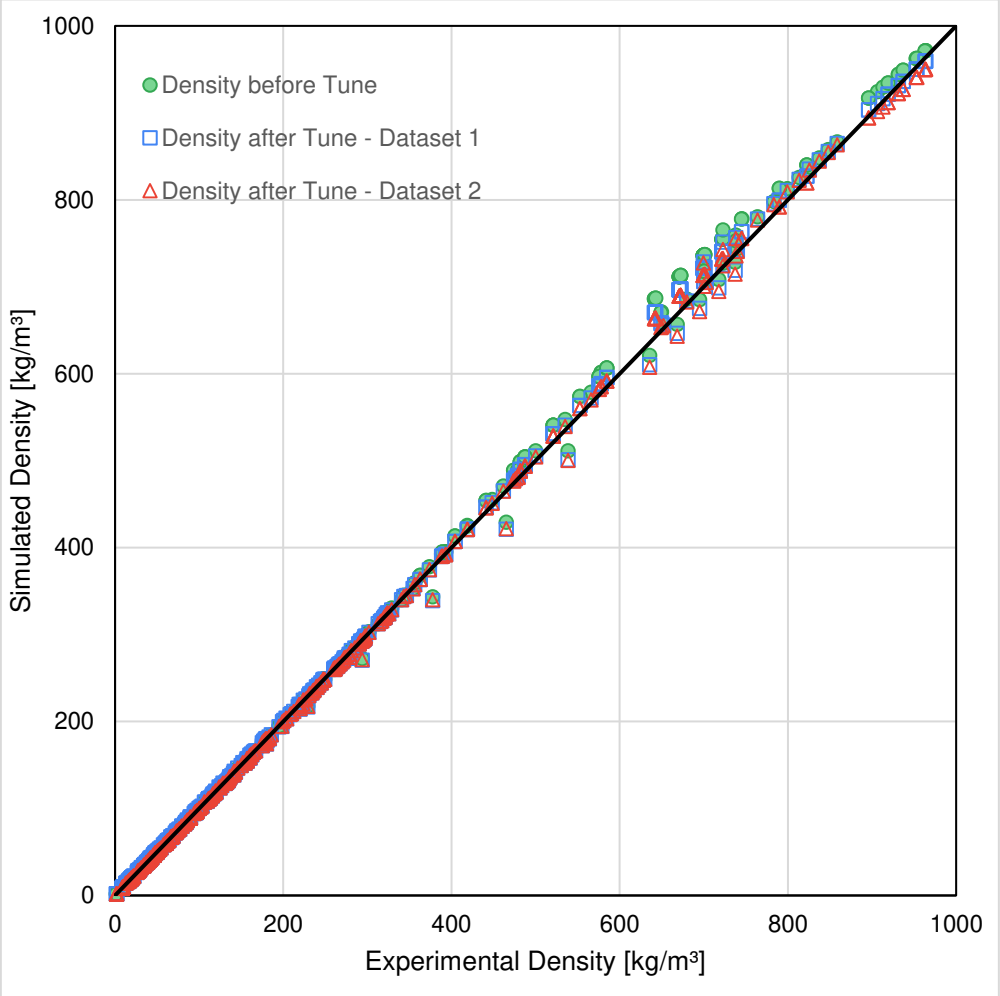

Source: Prepared by the author.

Furthermore, Figure B1 shows that the highest points on the graph had a more significant improvement, while for the lowest point, the adjustment did not demonstrate as much impact on the description of the densities.

The experimental data collected for $CO_2 + Ar$ mixture includes only impurity concentration values greater than 3%. Table B4 presents a comparison of statistical errors for several molar fraction ranges of Ar, before and after the tune of GERG-2008 for each dataset, considering training and validation data.

Table B4 – Average error values for the $CO_2 + Ar$ data for each impurity molar fraction before and after the GERG-2008 tuning. The best results are highlighted in bold. Calculated errors based on density values.

Ar molar fraction [%]	Num. of data	ARE [%]		MAE [kg/m^3]		RMSE [kg/m^3]	
		Before	After	Before	After	Before	After
Dataset 1							
3% up to 5%	43	0.933	**0.871**	4.662	**3.919**	67.731	**49.399**
5% up to 10%	7	0.392	**0.383**	0.144	**0.140**	0.050	**0.047**
10% up to 17%	96	1.467	**1.403**	**3.551**	3.612	**55.753**	83.912
Dataset 2							
3% up to 5%	43	0.933	**0.770**	4.662	**3.452**	67.731	**41.587**
5% up to 10%	7	**0.392**	0.400	**0.144**	0.147	**0.050**	0.052
10% up to 17%	96	1.467	**1.431**	**3.551**	3.740	**55.753**	90.637

Source: Prepared by the author.

For dataset 1, the 3% up to 5% Ar concentration range yielded a good result compared to other concentration levels with de tune model. This trend was even more evident in the tuning of dataset 2. Given that, this concentration range is typical in CCUS processes (Table 1), these findings are particularly significant. For the remaining concentration ranges, the adjustments made to the model did not lead to a noticeable improvement in performance. The range of 5% up to 10% was the one that presented the smallest errors; however, it is the one with the least experimental data being considered in the analysis.

Regarding the determination of the critical point, the tune of both dataset presents values very close to those of the original model (Table B5).

Table B5 – Simulated critical points before and after the adjustments of the GERG-2008 model for the $CO_2 + Ar$.

Ar molar [%]	Original Before tune		Dataset 1 After tune		Dataset 2 After tune	
	T_C [K]	P_C [MPa]	T_C [K]	P_C [MPa]	T_C [K]	P_C [MPa]
3%	303.824	8.072	303.837	8.097	303.750	8.080
5%	303.112	8.456	303.098	8.492	302.951	8.463
15%	297.297	10.154	297.063	10.235	296.629	10.146
25%	288.834	11.753	288.273	11.888	287.612	11.742

Source: Prepared by the author.

The model tuned allowed a fine adjustment in relation to the density prediction without generating significant changes in the definition of the critical points for all Ar molar fraction analyzed in the Table B5.

In addition, the model adjustment that proved to be most efficient based on the validation data was the one that used dataset 2. In general, the GERG-2008 tuned for $CO_2 + Ar$ is recommended, since there was a significant reduction in the MAE and RMSE values for the considered experimental densities.

B.2 EOS-CG 2019

Since the GERG-2008 formulation, more precise experimental data for the $CO_2 + Ar$ system have been available, enabling EOS-CG 2019 to achieve a more sophisticated tune for this binary mixture. Another improvement compared to GERG-2008 is the definition of the departure function formulation, which is already adjusted using these new experimental data and set as unity (Herrig, 2018). Therefore, it is expected that the model describes the system very well, but an investigation into the refinement of F_{ij}, for example, is valid.

Simulation of two training data group identified dataset 2 as having the lowest average errors (Table B6). Analysis of the errors of adjusted parameter combinations revealed a greater impact of temperature parameters (β_T and γ_T) on model results compared to volume parameters (β_v and γ_v) upon tuning. This was also observed for departure function adjustments, where combinations containing with F_{ij} has a greater improvement.

Table B6 – Performance of fitting parameters combinations of EOS-CG 2019 for $CO_2 + Ar$ training set (369 data). The combinations of adjustment are identified in the Table 5. The best results are highlighted in bold. Calculated errors based on density values.

Combination of adjustment [-]	Dataset 1			Dataset 2		
	ARE [%]	MAE $[kg/m^3]$	RMSE $[kg/m^3]$	ARE [%]	MAE $[kg/m^3]$	RMSE $[kg/m^3]$
1	**0.566**	1.961	5.206	0.566	1.962	5.208
2	1.299	5.598	12.350	1.054	4.665	10.026
3	0.647	2.187	6.276	0.647	2.187	6.276
4	0.855	4.026	8.036	0.772	3.465	7.065
5	**0.566**	**1.957**	**5.204**	**0.565**	**1.955**	**5.197**
6	1.010	4.178	9.023	1.145	5.502	11.958
7	1.118	5.578	11.116	0.791	3.589	7.269
Average ARE	0.866	3.641	8.173	**0.791**	**3.332**	**7.571**

Source: Prepared by the author.

Combination 5, exhibiting the lowest error for both datasets and was selected to determine the new adjustable parameters for EOS-CG 2019. This choice is based on its adjustment of only the temperature terms (previously shown to have a greater performance impact than volume terms) and the F_{ij} term (fixed at 1 in the original model). The parameters values before and after tuning are presented in Table B7.

Table B7 – The values of the adjustable parameters for EOS-CG 2019 for $CO_2 + Ar$ after the tuning process.

Parameters	Before tune	Dataset 1	Dataset 2
		After tune	After tune
$\beta_{T,ij}$	0.9987050	-0.0161825	-0.0148052
$\gamma_{T,ij}$	1.0396748	0.9559781	0.9569955
$\beta_{v,ij}$	1.0037659	1.0037659	1.0037659
$\gamma_{v,ij}$	1.0138330	1.0138330	1.0138330
F_{ij}	1	0.9939209	0.9753979

Source: Prepared by the author.

$\beta_{T,ij}$ was the parameter with the most significant change in value. While $\gamma_{T,ij}$ and F_{ij} were also adjusted, the changes were minor. However, these small adjustments were enough to produce a slight improvement, over the original model (a reduction of 0.11% in the ARE) for validation set, as shown in Table B8.

Table B8 – Error values calculated for the validation set (121 data) of the $CO_2 + Ar$ mixture for the EOS-CG 2019. The best results are highlighted in bold. Calculated errors based on density values.

	Validation set 1		Validation set 2	
	Before tune	After tune	Before tune	After tune
ARE [%]	0.632	**0.521**	0.632	**0.520**
MAE [kg/m^3]	2.552	**1.712**	2.552	**1.709**
RMSE [kg/m^3]	5.817	**4.348**	5.817	**4.329**

Source: Prepared by the author.

The results after tuning for the validation sets were almost the same. A slight improvement was observed in the reduction of MAE and RMSE. These results reinforce again the fact that the experimental data are not biased. For the $CO_2 + Ar$ mixture, the EOS-CG 2019 already describes the density very well, as can be seen in Figure B2, as well as the proximity of the performance of both dataset adjustments, as said.

Figure B2 – Simulated density versus experimental density for the system $CO_2 + Ar$ using the fitted model of the EOS-CG 2019.

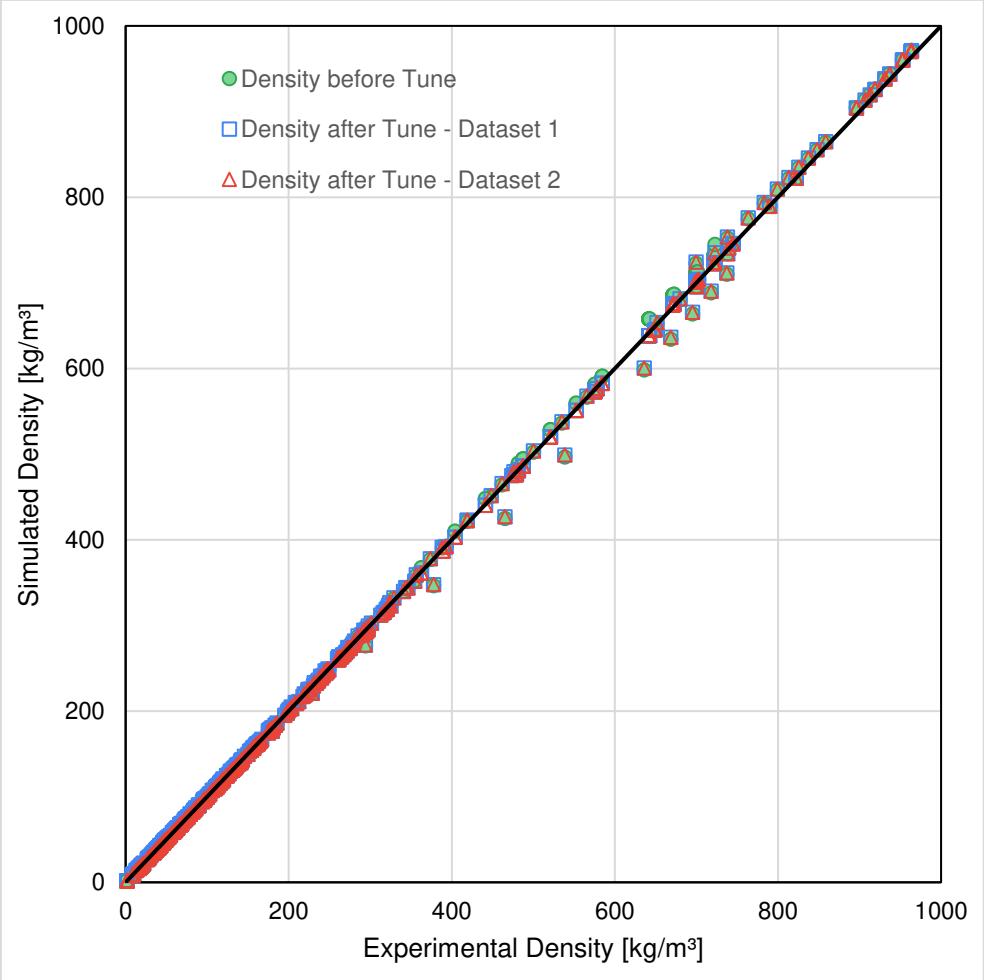

Source: Prepared by the author.

An individual analysis of the tunes quality by reference to the experimental data demonstrated that the tuned model obtained a more significant improvement in the prediction capacity of the experimental densities than the original model for the data of Kestin; Kobayashi; Wood (1966) for 50.025% Ar molar fraction.

Table B9 shows that the adjustments were efficient for the Ar molar fraction ranges between 3% and 5%, reducing ARE values by almost half and a good reduction in the RMSE value. For the other ranges, the original model has smaller errors than the tuned one, but they are still quite similar, indicating that for these concentration ranges the original version would already be sufficient. The RMSE value for 10% up to 17% Ar range had a significant increase after tune, which may be an indication that the model was not able to predict the outliers.

Table B9 – Average error values for the $CO_2 + Ar$ data for each impurity molar fraction before and after the EOS-CG 2019 tuning. The best results are highlighted in bold. Calculated errors based on density values.

Ar molar fraction [%]	Num. of data	ARE [%]		MAE [kg/m^3]		RMSE [kg/m^3]	
		Before	After	Before	After	Before	After
Dataset 1							
3% up to 5%	43	0.933	**0.447**	4.662	**2.925**	67.731	**36.727**
5% up to 10%	7	**0.392**	0.487	**0.144**	0.183	**0.050**	0.079
10% up to 17%	96	**1.467**	1.562	3.551	**4.160**	**55.753**	94.854
Dataset 2							
3% up to 5%	43	0.933	**0.444**	4.662	**2.922**	67.731	**36.754**
5% up to 10%	7	**0.392**	0.491	**0.144**	0.185	**0.050**	0.080
10% up to 17%	96	**1.467**	1.570	**3.551**	4.178	**55.753**	93.933

Source: Prepared by the author.

The determination of critical pressures and temperatures (Table B10) does not show divergence either between the tune with one dataset and another dataset, or between the original and tuned model regardless of the molar fraction of Ar.

Table B10 – Simulated critical points before and after the adjustments of the EOS-CG 2019 model for the $CO_2 + Ar$.

Ar molar [%]	Original Before tune		Dataset 1 After tune		Dataset 2 After tune	
	T_C [K]	P_C [MPa]	T_C [K]	P_C [MPa]	T_C [K]	P_C [MPa]
3%	302.831	7.898	302.792	7.874	302.769	7.869
5%	301.403	8.164	301.357	8.125	301.319	8.115
15%	293.157	9.418	293.294	9.379	293.218	9.356
25%	283.746	10.784	284.479	10.853	284.416	10.822

Source: Prepared by the author.

In summary, the tune of the EOS-CG 2019 model for $CO_2 + Ar$ mixture using data from dataset 2 yielded the lowest statistical error values as shown in Table B8. Although it reduced the ARE value, the impact of the adjustment was not very significant, but it can be applied if a more refined prediction of densities is needed, especially for the range of 3% up to 5% Ar as impurity.

APPENDIX C - CARBON DIOXIDE + METHANE SYSTEM ($CO_2 + CH_4$)

C.1 GERG-2008

In the case of the $CO_2 + CH_4$ mixture, the original GERG-2008 is configured with reducing function fitted to the binary mixture and a specific departure function where F_{ij} is set to 1 (Kunz and Wagner, 2012). The influence on the refinement of the reduction functions and/or F_{ij} can be evaluated in order to understand the feasibility of improving the model's prediction capacity.

Based on average errors of Table C1, dataset 1 demonstrated the best performance among the dataset 2. Analysis of the adjustments revealed that combinations 3, 4 and 7 exhibited errors values exceeding those of the original model (no tune) for this dataset (ARE of 3.580% and MAE of 18.917 kg/m^3).

Table C1 – Performance of fitting parameters combinations of GERG-2008 for $CO_2 + CH_4$ training set (132 data). The combinations of adjustment are identified in the Table 5. The best results are highlighted in bold. Calculated errors based on density values.

Combination of adjustment	Dataset 1			Dataset 2		
	ARE [%]	MAE $[kg/m^3]$	RMSE $[kg/m^3]$	ARE [%]	MAE $[kg/m^3]$	RMSE $[kg/m^3]$
1	**3.056**	**17.147**	**26.928**	**3.127**	**17.171**	**26.544**
2	3.539	18.975	28.603	3.759	19.585	29.823
3	3.927	21.088	30.461	4.501	23.862	34.613
4	3.740	21.126	29.162	3.849	20.725	28.940
5	3.127	17.615	27.118	3.146	17.271	26.546
6	3.473	18.749	28.435	3.711	19.411	29.649
7	3.712	20.954	29.012	3.842	20.665	28.882
Average ARE	**3.512**	**19.395**	**28.531**	3.704	20.097	29.286

Source: Prepared by the author.

Despite the potential for improvement by adjusting the F_{ij} parameter, simulations indicated a negligible impact on the results (combination 3 and comparison between combinations 1 with 5). Furthermore, it was noted that the adjustment in $\beta_{T,ij}$ and $\gamma_{T,ij}$ are more significant in reducing statistical errors when compared to the adjustments of $\beta_{v,ij}$ and $\gamma_{v,ij}$.

Seeking a balance between good model fit and computational efficiency, the adjustment of combination 1 was implemented for both datasets. The Table C2 shows the new parameters for tuned GERG-2008.

Table C2 – The values of the adjustable parameters of the GERG-2008 for $CO_2 + CH_4$ after the tuning process.

Parameters	Before tune	Dataset 1	Dataset 2
		After tune	After tune
$\beta_{T,ij}$	0.97787654	-0.05529325	-0.05644778
$\gamma_{T,ij}$	0.97566539	0.96582317	0.95865732
$\beta_{v,ij}$	1.00048208	1.00048208	1.00048208
$\gamma_{v,ij}$	1.00280702	1.00280702	1.00280702
F_{ij}	1	1	1

Source: Prepared by the author.

As in the previous model, $\beta_{T,ij}$ was the parameter that changed the most (reduction of, on average, 105.71%), while $\gamma_{T,ij}$ term had an adjustment of only 1.38%, on average. Even adjusting only $\beta_{T,ij}$ and $\gamma_{T,ij}$ terms shows an improvement in the model reaching almost 1.18% in the ARE for validation data for dataset 1, as evidenced by Table C3.

Table C3 – Error values calculated for the validation set (46 data) of the $CO_2 + CH_4$ mixture for the GERG-2008. The best results are highlighted in bold. Calculated errors based on density values.

	Dataset 1		Dataset 2	
	Before	After	Before	After
ARE [%]	3.985	**2.806**	3.357	**3.043**
MAE [kg/m^3]	22.835	**17.785**	20.439	**19.954**
RMSE [kg/m^3]	34.148	**28.667**	30.484	**30.293**

Source: Prepared by the author.

The fitted GERG-2008, when applied to the full dataset for the $CO_2 + CH_4$ mixture, shows a more significant improvement for the data corresponding to tune of dataset 1, while the Figure C1 shows that dataset 2 looks similar to the points generated by GERG-2008 without adjustment.

Figure C1 – Simulated density versus experimental density for the system $CO_2 + CH_4$ using the fitted model of the GERG-2008.

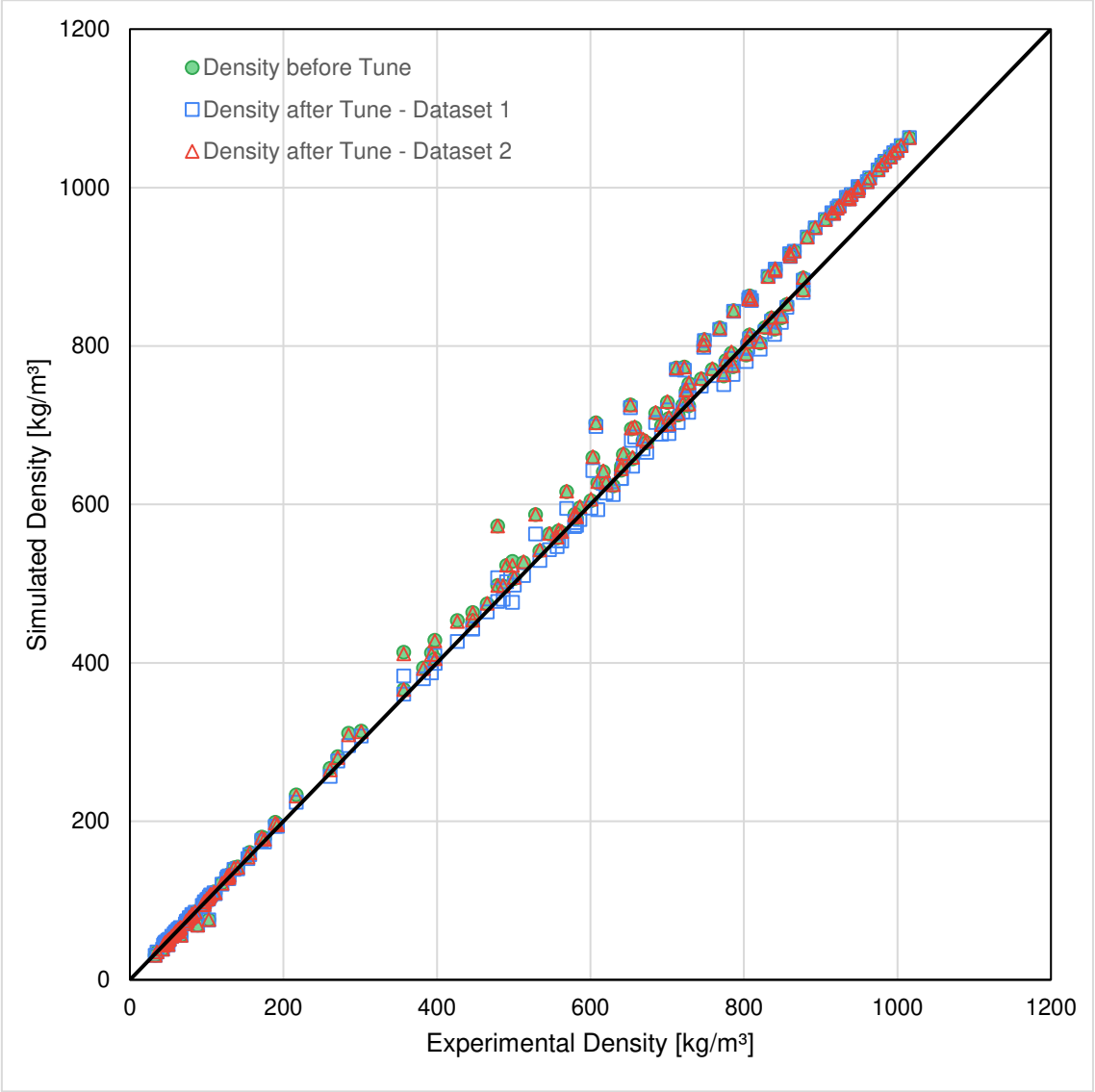

Source: Prepared by the author.

In Figure C1, at the top, there is a set of data aligned systematically away from the reference line. This set is the data from AL-SIYABI (2013), with CH_4 concentrations ranging from 0.10% to 2.50%, and they performed below the rest of the data.

By applying the tune of each dataset to the complete database and analyzing some ranges of molar fraction of impurity CH_4, as shown in Table C4, it was noted that for concentrations lower than 3%, dataset 1 was able to have an adjustment, albeit small, and for the range of 3% to 5%, this did not happen. For dataset 2, this behavior is the opposite.

Table C4 - Average error values for the $CO_2 + CH_4$ data for each impurity molar fraction before and after the GERG-2008 tuning. The best results are highlighted in bold. Calculated errors based on density values.

CH_4 molar fraction [%]	Num. of data	ARE [%]		MAE [kg/m^3]		RMSE [kg/m^3]	
		Before	After	Before	After	Before	After
				Dataset 1			
0% up to 1%	30	5.752	**5.726**	52.038	**51.818**	2721.414	**2697.327**
1% up to 3%	11	8.260	**7.948**	60.094	**57.887**	3776.560	**3497.077**
3% up to 5%	5	**0.604**	0.668	**5.170**	5.752	**34.370**	40.287
				Dataset 2			
0% up to 1%	30	**5.752**	5.758	**52.038**	52.086	**2721.414**	2726.656
1% up to 3%	11	**8.260**	8.286	**60.094**	60.294	**3776.560**	3799.787
3% up to 5%	5	0.604	**0.590**	5.170	**5.043**	**34.370**	35.680

Source: Prepared by the author.

Regarding the prediction of critical points, dataset 1 returned critical pressures closer to those generated by the original GERG-2008. Furthermore, for both datasets, the critical temperatures for higher concentrations (15% and 25%) returned lower critical temperatures than those of the EOS without tuning. In any case, the values obtained were still quite similar to each other, without major deviations, except for the case of 25% of CH_4 where for both dataset 1 and dataset 2 the critical temperatures is lower by almost 1K.

Table C5 – Simulated critical points before and after the adjustments of the GERG-2008 model for the $CO_2 + CH_4$.

CH_4 molar [%]	Original Before tune		Dataset 1 After tune		Dataset 2 After tune	
	T_C [K]	P_C [MPa]	T_C [K]	P_C [MPa]	T_C [K]	P_C [MPa]
3%	302.188	7.644	302.396	7.742	302.450	7.766
5%	300.731	7.793	300.959	7.934	301.026	7.970
15%	292.289	8.372	292.182	8.627	292.204	8.709
25%	282.578	8.763	281.658	8.996	281.513	9.112

Source: Prepared by the author.

Overall, the GERG-2008 adjustment for the $CO_2 + CH_4$ mixture proved to be more effective for dataset 1 (Table C3). However, the original version of the model yields a good result.

C.2 EOS-CG 2019

When modeling the $CO_2 + CH_4$ mixture, EOS-CG 2019 adopts the same adjustable parameters as the reducing function used in GERG-2008, as well as the same specific departure function, $F_{ij} = 1$ (Herrig, 2018). Therefore, it also makes sense to evaluate whether an adjustment to the F_{ij} parameter would bring any more significant improvement. As evidenced by Table C6, dataset 1 once more exhibited the lowest mean errors and was thus selected as the basis for subsequent analyses.

Table C6 – Performance of fitting parameters combinations of EOS-CG 2019 for $CO_2 + CH_4$ training set (142 data). The combinations of adjustment are identified in the Table 5. The best results are highlighted in bold. Calculated errors based on density values.

Combination of adjustment [-]	Dataset 1			Dataset 2		
	ARE [%]	MAE $[kg/m^3]$	RMSE $[kg/m^3]$	ARE [%]	MAE $[kg/m^3]$	RMSE $[kg/m^3]$
1	3.448	19.504	31.567	3.399	19.216	31.354
2	3.536	19.148	28.714	3.558	19.065	28.675
3	3.949	21.168	30.548	4.331	23.439	32.858
4	3.766	21.312	32.279	4.012	22.520	33.102
5	3.238	18.322	27.636	**3.118**	17.594	27.088
6	**3.036**	**16.835**	**26.825**	3.155	**17.404**	**26.930**
7	3.808	21.719	30.452	4.015	22.483	30.983
Average	**3.605**	**19.814**	**30.467**	3.712	21.072	31.137

Source: Prepared by the author.

Investigating the combinations, it was noticed that the combinations involving F_{ij} showed in general, an improvement in error values. For the case in which the adjustment of the departure function is not taken into account (combinations 1 and 2), it was found that the parameters relating to temperature showed a slight improvement in terms of predicting densities. The opposite occurs when considering the adjustment of the F_{ij} term (combination 5 and 6), where the volume parameters perform better.

Combinations 3, 4 and 7, all exhibiting ARE values exceeding the original model value of 3.593% and were discarded. Combination 6, with adjustments made only to $\beta_{v,ij}$, $\gamma_{v,ij}$ and F_{ij}, ultimately demonstrated the lowest errors, thus

being selected for subsequent analyses for both datasets. The new model parameters are listed in Table C7.

Table C7 – The values of the adjustable parameters of the EOS-CG 2019 for $CO_2 + CH_4$ after the tuning process.

Parameters	Before tune	Dataset 1	Dataset 2
		After tune	After tune
$\beta_{T,ij}$	0.97787654	0.97787654	0.97787654
$\gamma_{T,ij}$	0.97566539	0.97566539	0.97566539
$\beta_{v,ij}$	1.00048208	-0.13740739	-0.12249178
$\gamma_{v,ij}$	1.00280702	0.92658400	0.92814207
F_{ij}	1	2.06507826	2.31514645

Source: Prepared by the author.

The largest adjustments were to the F_{ij} and $\beta_{v,ij}$ terms. In particular, the term of the departure function had an update in its value of, an average, of 119.01%. These adjustments resulted in a 1.02 percentage points improvement (Table C8) in the validation data for the $CO_2 + CH_4$ mixture.

Table C8 – Error values calculated for the validation set (36 data) of the $CO_2 + CH_4$ mixture for the EOS-CG 2019. The best results are highlighted in bold. Calculated errors based on density values.

	Dataset 1		Dataset 2	
	Before tune	After tune	Before tune	After tune
ARE [%]	3.987	**2.962**	4.010	**2.947**
MAE [kg/m^3]	22.834	**18.303**	22.934	**18.056**
RMSE [kg/m^3]	34.132	**29.087**	34.217	**28.694**

Source: Prepared by the author.

The tune using dataset 2 had a greater reduction in errors compared to the original model. In Figure C2, the good quality of the adjustments is evident, especially for the experimental points in the central region of the graph. In both datasets, the performances are similar, with the tuning of dataset 2 being slightly better than dataset 1 for the complete experimental dataset.

Figure C2 – Simulated density versus experimental density for the system $CO_2 + CH_4$ using the fitted model of the EOS-CG 2019.

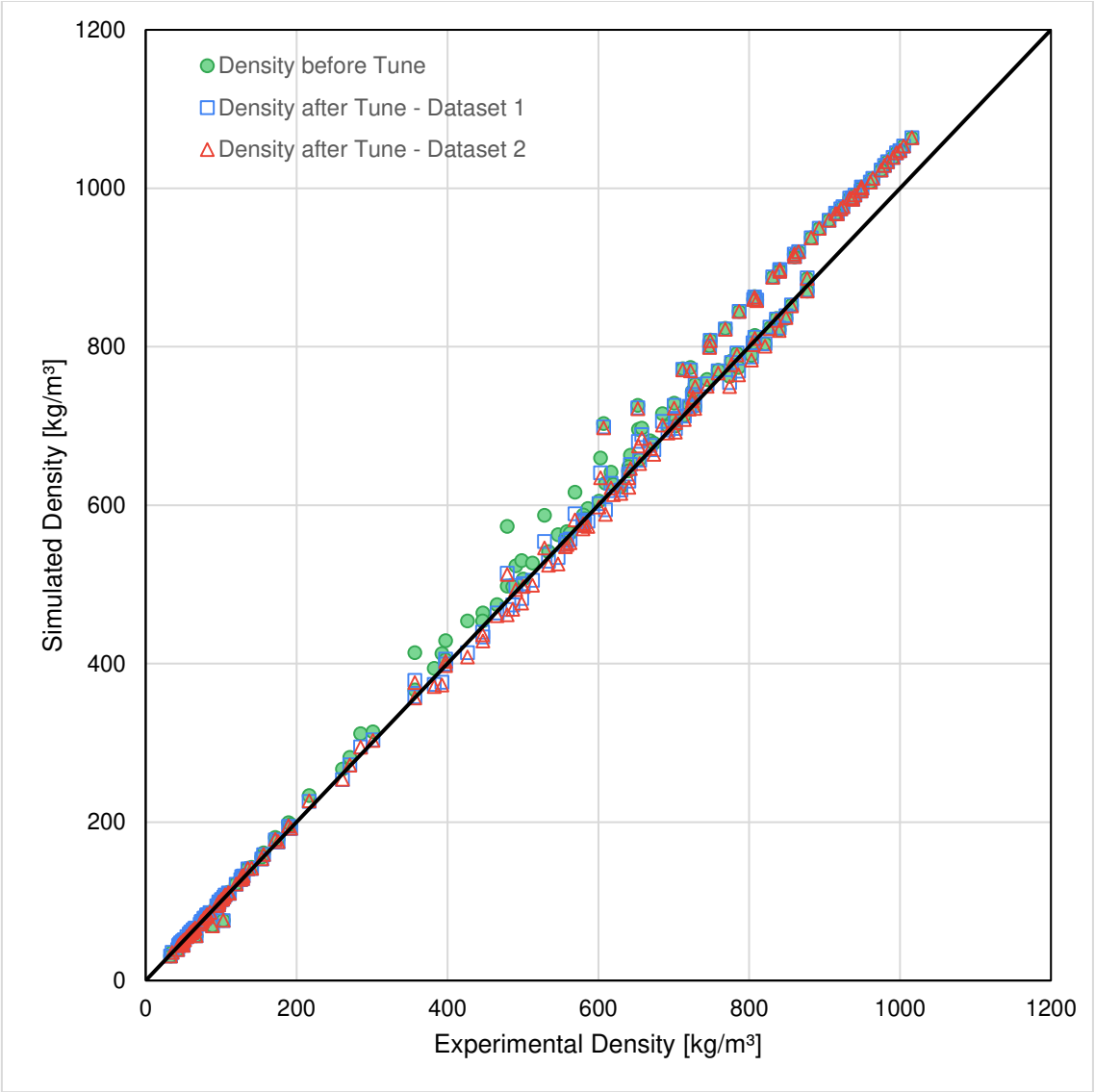

Source: Prepared by the author.

In the Figure C2 there is a region where the tunes show an improvement in the predictive capacity of densities, with the points coming from Arai; Kaminishi; Saito (1971).

Based on the analysis of the tunes of each of the datasets by impurity concentrations ranges, it was observed that 1% to 3% and 3% to 5% CH_4, the adjusted models presented better performance than their original version (Table C9). In addition, the last range studied was the one with the lowest error values. However, it is worth noting that there were only 5 experimental data available for this analysis, which may influence the statistical results.

Table C9 – Average error values for the $CO_2 + CH_4$ data for each impurity molar fraction before and after the EOS-CG 2019 tuning. The best results are highlighted in bold. Calculated errors based on density values.

CH_4 molar fraction [%]	Num. of data	ARE [%]		MAE [kg/m^3]		RMSE [kg/m^3]	
		Before	After	Before	After	Before	After
Dataset 1							
0% up to 1%	30	**5.587**	5.599	**51.527**	51.632	**2665.448**	2676.327
1% up to 3%	11	8.261	**8.075**	60.097	**58.851**	3777.518	**3602.333**
3% up to 5%	5	0.609	**0.582**	5.205	**5.005**	34.434	**32.810**
Dataset 2							
0% up to 1%	30	**5.587**	5.594	**51.527**	51.591	**2665.448**	2671.898
1% up to 3%	11	8.261	**7.978**	60.097	**58.160**	3777.518	**3517.306**
3% up to 5%	5	0.609	**0.604**	**5.205**	5.207	34.434	**33.049**

Source: Prepared by the author.

The tuned models returned lower values of temperature and critical pressure for all concentrations analyzed, as seen in Table C10. Dataset 1 has values closer to those of the original EOS-CG 2019, especially for critical pressures. Critical temperatures are the ones that present the greatest deviations when compared to the original model, especially in dataset 2, where for 25% CH_4 it returned 4K less (for this same concentration, the tune of dataset 1 returns almost 3K less).

Table C10 – Simulated critical points before and after the adjustments of the EOS-CG 2019 model for the $CO_2 + CH_4$.

CH_4 molar [%]	Original Before tune		Dataset 1 After tune		Dataset 2 After tune	
	T_C [K]	P_C [MPa]	T_C [K]	P_C [MPa]	T_C [K]	P_C [MPa]
3%	302.256	7.648	301.822	7.644	301.611	7.615
5%	300.755	7.789	300.067	7.787	299.730	7.744
15%	292.052	8.342	290.110	8.327	289.399	8.215
25%	282.230	8.743	279.245	8.700	278.108	8.515

Source: Prepared by the author.